Final Technical Report

Cooperative Agreement NCC 3-59
"Interfacial Bond Characterization Ceramic/Ceramic Composites"

Submitted to:

NASA
Lewis Research Center
Cleveland, Ohio 44135

Submitted by:

Dr. James Laughner
New York State College
of Ceramics at Alfred University
Alfred, NY 14802

PREPARATION AND EVALUATION OF SILICON NITRIDE MATRICES
FOR SILICON NITRIDE - SiC FIBER COMPOSITES

BY

Scott R. Axelson

A THESIS
SUBMITTED TO THE FACULTY OF
ALFRED UNIVERSITY
IN PARTIAL FULFILLMENT OF THE REQUIREMENTS
FOR THE DEGREE OF

MASTER OF SCIENCE
IN
CERAMIC SCIENCE

ALFRED, NEW YORK

FEBRUARY 1988

Contents

ACKNOWLEDGEMENTS

ABSTRACT

The need for high temperature, high strength materials for advanced engineering applications has provided the driving force for research and development of ceramic matrix composites. Although reduction and control of the flaw size in a ceramic offers increases in the strength, fracture toughness remains approximately the same. The inclusion of second phases (whiskers, fibers, or a material that undergoes a phase transformation) causes significant changes in the mechanical properties over a monolithic material. Second phases allow the local dissipation of strain energy as cracking occurs, altering or inhibiting further crack propagation until higher stresses are applied. Increased resistance to catastrophic failure results, raising the fracture toughness of the ceramic.

This research deals with the addition of continuous silicon carbide (SiC) fiber to three types of silicon nitride (Si_3N_4) matrices. Efforts were aimed at producing a dense Si_3N_4 matrix from reaction-bonded silicon nitride (RBSN) by hot-isostatic-pressing (HIP) and pressureless sintering, and from Si_3N_4 powder by hot-pressing. The sintering additives utilized were chosen to allow for densification, while not causing severe degradation of the fiber. The ceramic microstructures were evaluated using scanning optical microscopy. Vickers indentation was used to determine the microhardness and fracture toughness values of the matrices.

The RBSN matrices in this study did not reach more than 80% of theoretical density after sintering at various temperatures, pressures, and additive levels. Hot-pressing Si_3N_4 powder produced the highest density matrices; hardness and toughness values were within an order of magnitude of the best literature values. The best sintering aid composition chosen included Y_2O_3, SiO_2, and Al_2O_3 or AlN. Photomicrographs demonstrate a significant reduction of fiber attack by this additive composition.

vi

Chapter 1

Introduction

1.1 Background

Ceramic matrix composite (CMC) materials have become one of the most actively researched areas in ceramics. This class of structural materials has application where high strength, high toughness. low thermal expansion, low density, high-temperature stability, and corrosive environment stability are desirable. The major advantage is that the presence of the ceramic fibers can prevent catastrophic failure by allowing for the dissipation of fracture energy as cracking occurs.

Structural composites are currently being developed that can withstand high temperature environments as high as 2200°C; others are needed for the high-stress utilization in new turbine engines, such as the AGT-101 [1]. Cutting tools composed of CMC are available commercially for use on metal alloys and medium density fiberboard (MDF) [2]. Other applications for structural CMC will develop as raw material and fabrication costs decrease.

Major research and development resources have been devoted towards the advancement of nitrides and carbides as structural materials. These systems have been sintered. hot-pressed. and hot-isostatically-pressed (HIP) to attempt to achieve near theoretical density and strength. However, even with these advancements, monolithic pieces still have relatively low toughness compared to metal alloys and fail catastrophically rather than undergo deformation.

The introduction of homogeneously distributed, second phase materials to carbide or nitride matrices provides higher values of toughness for the composite. Research efforts at NASA-Lewis have centered on the inclusion of continuous fibers in a ceramic matrix. Reaction-bonded silicon nitride (RBSN) is a choice matrix, primarily due to characteristically low shrinkage ($\leq$ 10%) from the precursor silicon powder to the final densified piece.

1.2 Objectives

The objective of the present study was to examine different Si_3N_4 matrices for use in CMC, based upon their sintered densities, microstructures, and the mechanical properties of hardness and toughness. In addition, sections of SiC fibers placed in each matrix were examined to give qualitative observations of the effect of sintering temperature and additives on any reaction between the fiber and matrix. Three different densified Si_3N_4 matrices were prepared and characterized in this investigation: (1) Matrix 1: HIP'd RBSN. (2) Matrix 2: Pressureless Sintered RBSN. and (3) Matrix 3: Hot-Pressed Si_3N_4. Since Si_3N_4 decomposes at typical sintering temperatures. a triple oxide sintering aid composition was used in order that a liquid would form at temperatures within 300°C of the nitriding temperature.

The levels of Y_2O_3 utilized for the formation of Matrix 2 were based upon observations made by researchers at Ford [3,4.5]; the addition of fibers added a new facet to pressureless sintered RBSN. Various temperatures and additive percentages were chosen to evaluate their effect on the fiber-matrix interface. The type and concentration of sintering additive alter the interfacial chemical reaction.

Based on the SRBSN matrices, the decision was made to look at a dense matrix made from hot-pressed Si_3N_4. The triple oxide additive was chosen for use in the HIP matrices in order to allow correlations to be made between Matrix 1 and Matrix 3. The Y-SiAlON composition was chosen as an additive for hot-pressing since this liquid phase, shown to crystallize at the grain boundary, was expected to have a higher toughness and refractoriness due to the presence of nitrogen in the structure [6,7].

Chapter 2

Literature Survey

2.1 Introduction

Ultimately, all the applications of Si_3N_4 depend upon the molecular structure; properties like band gap, diffusion, thermal expansion, and hardness are affected by bond types, bond length and angles, band structure, and the crystal system. Besides the amorphous phase produced in the plasma-enhanced, chemical vapor deposition (CVD) process, β and α crystal modifications are the only two polymorphs of Si_3N_4 known to exist. Turkdogan, Bills, and Tippet [8] first established the existence of the two forms, claiming them to have identical compositions, Si_3N_4. Hardie and Jack [9] showed both forms to be hexagonal, with α having a c-dimension twice that of β. It is generally believed that α is a low-temperature form and β a high-temperature form; however, both phases are usually formed at nitriding reaction temperature.

Grieveson, Jack, and Wilde [10] have suggested that α is a "high oxygen potential" form and β is the "low oxygen potential" form. It was suggested that the $\alpha-$phase was an oxynitride with the composition $Si_{11.5}N_{15}O_{0.5}$, where oxygen stabilizes the structure. Later work [11,12,13] shows that the oxygen content is not high enough in the α-phase for it to be a stoichiometric oxynitride with oxygen replacing N atoms in specified sites, although some oxygen may be contained as an impurity. Additional background and references may be found in a paper written for G.S.Fischman at Alfred on the electronic and crystal structure of silicon nitride [14].

2.2 Reaction-Bonded Si_3N_4

The reaction-bonding process is used to either produce a final monolithic product, a matrix for a composite, or to form the precursor for a fully dense material. Reaction-bonded silicon nitride (RBSN) has the properties necessary for high-performance applications: good thermal shock and

chemical corrosion resistance, low thermal expansion ($3 \times 10^{-6}/{}^\circ C$), 0.1% dimensional change during reaction, and high temperature mechanical strength [15].

Initial interest in RBSN resulted from the need to find materials that could withstand the higher operating temperatures present in new gas turbine engines. Increased operating temperatures improve the thermodynamic efficiency of an engine (fuel savings of 40% when operating at 1370°C rather than 1050°C) [16]; at the same time, however, the materials have to be lighter and inexpensive to produce (cost effective compared to present engine technology). Ford and Garrett Research have been working together to build a gas turbine utilizing stator vane segments. rotors (turbines), regenerator shields, bearings, and bolts composed of RBSN [1]. Other applications include thermocouple sheaths in corrosive environments, inert-gas welding torch nozzles. metalworking tools for drawing wire or grinding, cutting tools, heat exchangers, and radomes for the military.

2.2.1   Nitridation Reactions

Thermodynamic Calculations

Moulson [16] and Lindley et al. [17] have suggested that hydrogen aids in the removal of an oxide layer present on the silicon particles and increases the reaction rate, but the actual reaction mechanism has not yet been determined. Accurate thermodynamic data, however, can be utilized to calculate equilibrium compositions for all the possible compositions in the system and determine how the system adapts to changing reaction conditions: Shaw [18] performed the calculations for the nitridation of silicon. Two types of systems were considered in the calculations: $SiO_2/N_2/H_2$, where no Si is exposed to the atmosphere, and $Si/N_2/H_2/O_2$. The results of thermodynamic calculations show that H_2 does enhance the removal of the SiO_2 layer and increase the partial pressures of SiO. Si. and H_2O in the $SiO_2/N_2/H_2$ system. producing some Si_3N_4. For the $Si/N_2/H_2/O_2$ system. H_2 content in general has negligible effect.

Reaction Models

Several models have been proposed for the nitridation of silicon. Moulson describes the reaction as consisting of three stages with differing rate kinetics as shown in Figure 1. Linear kinetics are observed in stage 1 during the period of induction to remove the silica layer; there is a flux of oxygen-containing species away from the reaction surface. In stage 2 the reaction rate decreases with the amount of Si (approximately a $T^{1/2}$ dependence). Pore closure occurs as a nitride layer covers any remaining unreacted Si (approx. 2%), signifying stage 3 and no further reaction in the system.

Silicon metal particle size affects the reaction rates and mechanisms. Particles greater than 10 μ inhibit the nitridation process and increase the chance of unreacted Si remaining in the

4

structure. At temperatures above the melting point of Si (1410°C), the liquid metal moves through the RBSN network and voids form where the unreacted Si previously existed [19]. These voids are strength-limiting defects in the structure.

Chemical impurities in the powder alter the reactions that occur. Various transition metals have been added to enhance nitridation. These additives. such as the oxides of Fe, Ni, Mn, Co, and Cr, act to promote the removal of the silica film from the Si particles either by diffusing through or disrupting the oxide layer, resulting in the volatilization of the silica [20]. Iron has been shown to open channels through the developing nitride layer. In addition, the production of β-phase is promoted by iron. The Fe and Si combine to form liquids which melt at temperatures as low as 1208°C ($FeSi_2$). The amount of β-Si_3N_4 is directly proportional to the percentage of Fe in the system. Shaw reported in a recent NASA study that full nitridation was obtained at 1375°C in one fourth the time with 0.6 wt% Fe [18].

Nitriding atmosphere has a major effect on the rate of reaction and type of reaction products. Figure 2 shows the main mechanisms of microstructure formation attributed to the nitriding environment with special emphasis on the "flowing" 95%N_2/5%H_2 atmosphere (Fig. 2(c)) [17]. The partial pressure of N_2 is known to control the nucleation site density on the silicon surface, forming β-phase material on the Si as some of the oxide layer slowly dissociates in a flowing N_2 atmosphere (Fig. 2(a)). A static N_2 environment results in negligible breakdown of the silica film due to very slow diffusion of O_2 away from and N_2 through this region, shown in Figure 2(b). Due to its high thermal conductivity, helium has been introduced into the reaction gas at 1-2 vol% to act as a heat sink: removal of heat from the exothermic reaction assists in controlling the reaction temperature (preventing the melting of the starting powders [21]).

The presence of hydrogen in the nitriding atmosphere seems to significantly change the nitridation process, promoting the formation of Si_3N_4 by vapor phase reactions. The gaseous reaction favors the α-phase material. A high ratio of α/β is known to improve the mechanical properties of RBSN. The simplest reaction for the formation of α-Si_3N_4 is

$$3Si(g) + 2N_2(g) \rightarrow Si_3N_4(s) \tag{2.1}$$

in conditions where a few ppm of O_2 and H_2O are present. This reaction is quite slow due to the presence of the silica layer. The addition of H_2 causes two reactions to occur: the first,

$$SiO_2(s) + H_2(g) \rightarrow H_2O(g) + SiO(g) \tag{2.2}$$
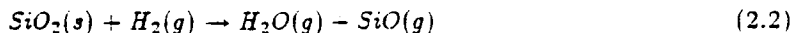
breaks up the nitrogen impervious silica film. Any O_2 impurity reacts with H_2 to from H_2O, decreasing the partial pressure of O_2 in the system. At all temperatures the H_2 in the nitridation gas increases the P_{SiO}, enabling α-phase to be formed

$$3SiO(g) + 2N_2(g) \rightarrow Si_3N_4(s) + 3/2O_2(g) \tag{2.3}$$
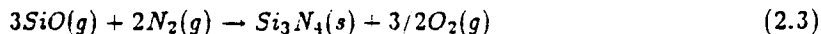
These two reactions, suggested by Lu and Riley [22], cause an increase in the nitridation rate because the H_2 acts as an oxygen sink in removing the SiO_2 and forming H_2O from impurity O_2 (there is an O_2 flux away from the nitride growth sites. A high P_{SiO} within the compact allows nearly complete nitridation to occur while preventing an nitrogen impervious Si_3N_4 film to from at the Si/SiO_2 interface.

The $Si(g)$ and $SiO(g)$ reactions allow nitridation to occur much more rapidly in the initial stages. Figure 3 shows the rate as a function of the fraction converted; the N_2/H_2 atmosphere definitely contributes to the rate at which RBSN is formed. The function of H_2 is very important early in the reaction, however. Other factors affect the nitridation of silicon. Recently, Rahaman and Moulson [23] noted that a pretreatment in hydrogen or argon affected the nitridation rate, shown in Figure 4. The silica layer was removed in half an hour in H_2 and after one hour in Ar, both at $1350°C$ at a gas flow rate of 0.1 - 0.5 l/min. The pretreatment resulted in considerably reduced times (less than two hours) to reach greater than 95% nitridation; a $N_2/5\%H_2$ atmosphere and H_2 pretreatment allowed nearly 100% reaction after 20 hr (with a high α/β ratio). The use of N_2 only and no pretreatment stage produced only 30% reaction after 24 hr.

As was previously stated, the 'mechanics' of the atmosphere seemed to change the quality of RBSN formed. A flowing nitrogen atmosphere resulted in a lower α/β ratio, probably due to the removal of vapor phase reactants (Si, SiO) from the sample: impurities may also be removed, while at the same time porosity formation is encouraged. A static N_2 atmosphere results in a more uniform product, but the reaction proceeds at a much slower rate. A study by Jones and Lindley [24] showed that H_2 in the nitriding atmosphere eliminated the differences in the materials produced under flowing or static conditions. The early formation of a fine, α-phase network due to the increased content of SiO minimizes the vapor transport losses.

An alternate model for the effect of H_2 on the nitridation process agrees with the concept of silica film removal, the disagreement being with the $SiO(g)$. Dervisbegovic and Riley [25] believe that $SiO(g)$ is not involved, and instead that the rate of formation of Si_3N_4 is mostly controlled by the rate at which Si vapor is released from the solid surface. This results from the highly exothermic nature of the nitridation reaction, requiring the adsorbed or colliding species to react at a solid surface which acts as a sink to remove heat from the reaction zone. Any free O_2 or SiO gas reacts with hydrogen, forming water and $Si(g)$, respectively, the Si then reacting to form Si_3N_4. Most recent work supports the nitridation of $SiO(g)$ argument, however.

A comment by Dervisbegovic and Riley [26] summarizes this section best: "Hydrogen is involved in the normal rate-controlling process, and its function is not solely that of aiding removal of the reaction-inhibiting SiO_2 film from the Si."

6

2.2.2 Processing

It is already clear that process variables change the structure and properties of RBSN, so a brief outline of the process is necessary. Silicon samples are fabricated from powders with a mean particle size less than 10 μ and high surface areas for more complete reaction. Impurities introduced during comminution may be removed by acid leaching. Up to 2% of Fe or Ni may be added to aid in the nitridation process (also aiding the removal of the silica film). The particle size range is optimized and the system milled to maximize homogeneity to allow for high packing densities (green densities of approx. 1.70 g/cc) when fabricating the required shape. Parts may be isostatically pressed (200 MN/m_2) or injection molded using techniques similar to those for plastics. Ford has patented a technique called fugitive wax slip casting, while slip casting of Si may also be performed utilizing the same method as in traditional clay or oxide systems [19]. Other forming techniques include extrusion and flame spraying. These shaped samples might next be 'pre-sintered' in argon or hydrogen at 1200"C to give the piece strength for machining to the required shape and dimensions.

The nitridation process is undertaken in an atmosphere-controlled furnace to prevent the introduction of oxygen and other gases which would inhibit the nitridation process. The samples are placed on Si_3N_4 setters on alumina boats or reticulated setters for complete exposure to the atmosphere. Furnaces are evacuated and backfilled three to five times with nitrogen or an inert gas to remove air from the chamber and from voids in the precursor samples. Nitridation reaction times and temperatures range from several hours to two days and from 1200" to 1550"C. Besides N_2 and H_2, up to 2% He is sometimes added to the nitriding gas to carry heat away from this exothermic reaction.

Rather than nitriding the Si powder at only one temperature, researchers have proposed multi-step or gas-consumption cycles to control the reaction. Messier and Wong [27] proposed a multiple temperature cycle with a maximum temperature of 1400"C. The schedule change increased the degree of nitridation of the sample to produce strengths that were 50% higher than than when samples were nitrided at a single temperature in the reaction range. Mustel et al. [28] described a technique whereby consistent nitridation of Si could be carried out through analysis of the exhaust gases. The temperature and gas supply to the reaction chamber were controlled by a microprocessor which made decisions based on the N_2 concentration exiting the reaction chamber. When the flow out was too low compared to the flow in, the reaction was consuming N_2 too rapidly according to the kinetics (programmed into the computer); the furnace temperature was then held constant by the controller until the gas consumption returned to below a preset level. The results showed a shorter reaction time (30 hr instead of 70 hr) and $\geq 98\%$ reaction. A more homogeneous microstructure was observed from this self-regulated procedure compared to conventional temperature-control techniques.

2.2.3 RBSN Morphology

Moulson states "the hypothesis is proposed that, during the formation of RBSN, the growth of $\alpha-Si_3N_4$ occurs by vapor-phase reactions."[16] the type of reaction promoted by H_2 below the melting point of Si (1410"C). Whisker or needle-like structures are characteristic of $\alpha-$phase material. In the presence of H_2 a skeletal Si_3N_4 network forms in the sample. a continuous bridging phase resulting from the $N_2 - SiO$ reaction (more than 80% $\alpha-Si_3N_4$). Although any pretreatment may cause grain growth before nitridation begins. H_2 in the atmosphere has been shown to lower any subsequent grain growth during reaction by inhibiting material transport across grain boundaries.

Improper nitriding conditions can result in unreacted Si in the final piece. During the reaction the piece should gain 66.7% weight as Si_3N_4 is formed from Si, but the usual gain is between 60 and 62% due to vapor phase losses. Figures 5 and 6 show the weight gain and α β ratio as a function of the H_2 content for 1200" and 1375"C, respectively. Alpha content increases with H_2 in both cases; weight gain is independent of H_2 at 1375"C, however [18].

The micrograph in Figure 7 shows the effect of pretreatment on the microstructure. The finer particle size sample, heated and nitrided in $N_2/4\%H_2$ at 1375"C for four hours. began nitriding at lower temperatures to form a fully-reacted, fine-grained $\alpha-$phase network with no large porosity. The second sample which experienced grain growth as it was heated in He did not react completely due to the larger grain size, regardless of the presence of H_2.

The series of micrographs in Figure 8 show the effect of the H_2 content at 1375"C for four hours on the microstructure of the fracture surface [18]. Grain size and porosity become finer with increasing H_2; this gas inhibits grain growth and increases the vapor species to produce uniformly distributed porosity. The $\alpha-$phase tends to fill the original pores in the compact as nitridation proceeds.

2.2.4 Properties

As is the case for the microstructure. hydrogen changes the properties of RBSN. Besides the nitridation conditions, the final density of RBSN depends on the green density of the Si sample - a lower green density with higher porosity requires a greater degree of nitridation to occur before the continuous network is established. Mangels [19] stated that better low and high temperature properties resulted from the network microstructure obtained when H_2 was in the nitriding atmosphere.

The strength of a porous product is known to be a function of nitrided density, pore size. and grain size. RBSN is also affected by the extent of the bridging Si_3N_4 and impurity inclusions or large voids, which in this system would be mainly unreacted Si. Lindley et al. [17] used the equation

$$2a = [\pi K_{IC}^2(1 - \nu^2)]/4\sigma^2 \tag{2.4}$$

to calculate the critical defect size using data values from a double torsion test (K_{IC} is the critical

8

stress intensity factor, ν is Poisson's ratio, and σ is the strength at fracture). The critical defect size (2a) is lower for samples reacted in $N_2/5\%H_2$ (static and flowing) and in static N_2 than flowing N_2 by more than a factor of two. Strength is therefore lower in the sample nitrided in the flowing N_2 atmosphere. The use of H_2 in the atmosphere seems to eliminate any strength differences between static and flowing conditions. Fine grain structure and elimination of strength-limiting defects result from a N_2/H_2 atmosphere.

Other properties are affected since it appears that H_2 causes impurities to diffuse to the grain boundaries, improving RBSN for use at low and high temperatures. The addition of only 1% H_2 increased the modulus of rupture (MOR) by more than 30% and decreased the steady-state creep rate by a factor of four at room temperature (Figure 9). The high temperature strength decreased for the N_2 only RBSN with temperature and some plasticity was observed: the N_2/H_2 material exhibited none of this behavior (Figure 10) [29]. The finer, more uniform structure of the N_2/H_2 RBSN is also less anisotropic.

2.3 Sintering of RBSN

Achieving a dense product from a Si_3N_4 powder is a serious fabrication problem. Hot-pressing the powder requires the addition of additives which degrade the high temperature properties, and restricts the product to simple shapes. Shapes pressed or cast from Si_3N_4 powder may be sintered to high densities, but shrink between 15-20%, limiting close control of dimensional tolerances; additives again affect the resulting properties. Hot-isostatic-pressing (HIP) reduces the amount of additives necessary to achieve full density, although the cost of the equipment and low throughput limit the usefulness of this method for commercial applications.

2.3.1 Sintering Models

Brook [30] states that there are basically three types of processes leading to the densification of ceramics: (1) **Vitrification**, where heat treatment results in the formation of a liquid phase sufficient to fill the pore space in the compact, (2) **liquid phase sintering**, where the liquid phase is insufficient to fill the pore space so that a change in shape of the grains is necessary to achieve full density, and (3) **solid state sintering**, where no liquid phase is present, resulting in densification by changes in grain shape. Vitrification, the least complex of the three processes to model, is not a factor in SRBSN.

Three stages are used to describe what happens in a shaped part as sintering occurs. In the first stage some particles rearrange in the first liquid formed due to capillary forces; neck formation between grains and limited densification begins. A continuous pore network forms during the intermediate stage of sintering, with the density increasing to more than 90% of theoretical by

9

elimination of porosity. Slight grain growth occurs at this stage. In the final stage surface porosity closes off and closed pores intersect the grain boundaries: exaggerated grain or pore growth may occur at this stage. Attaining full density is limited by the degree to which the pore gases may dissolve in the liquid phase or diffuse to the outside of the body.

2.3.2   RBSN Sintering Additives

Sintering Si_3N_4 to full density is difficult in the absence of additives due to the covalent nature of the bonding; the diffusivity is low at temperatures below the thermal decomposition temperature. The additives promote the formation of a liquid phase at a lower temperature (which wets RBSN surfaces), decreasing the vapor-condensation mechanisms leading to decomposition and increasing the grain boundary transport. The main factors influencing the final density of SRBSN are the decomposition of the Si_3N_4 (if any), loss of sintering aids to the environment, and porosity elimination. Decomposition and loss of sintering aids can be prevented by packing the reaction-bonded component in a Si_3N_4 powder containing the same sintering aids.

Commonly used sintering aids for RBSN are MgO. CeO_2. and Y_2O_3. Mangels and Tennenhouse [3] and Giachello and Popper [31] have shown that RBSN can be fabricated. without post-sintering distortion. to yield a ceramic with high strength and nearly full density. Additional improvements in this material may occur through the addition of toughening agents such as SiC fibers or whiskers.

2.4   Hot-Pressed Si_3N_4 (HPSN)

Another method for densifying Si_3N_4 is by the use of hot-pressing, the application of an external pressure on the material at high temperature to provide the driving force for densification. The material is 'forced' to densify at temperatures below where exaggerated grain growth may occur: maximized material properties are possible due to the high density and small grain sizes resulting from this technique. However, expensive, short-life dies for high temperature use make this process expensive.

2.4.1   Densification Kinetics

Without the presence of sintering aids, researchers showed that α-Si_3N_4 could not be densified below 1750"C; above this temperature, decomposition occurred and increased with temperature. By adding 5 wt% MgO, nearly full density was possible above 1450"C at rates that were temperature and pressure dependent. Two stages in the densification process were defined [32].

In the first stage, particles rearranged quickly once the pressure was applied (above 1550"C) to about 0.6 of theoretical density. A magnesium silicate liquid had formed between the MgO and

SiO$_2$ present as a film on the Si$_3$N$_4$ particles, allowing a liquid-enhanced rearrangement with voids filled by the liquid. Limited particle deformation also occurred at local regions of high stress. The $\alpha \to \beta$ transformation was insignificant at this stage. Further densification was not possible at this stage without a higher additive concentration.

The second stage involves particle deformation to reach densities between 0.65 and 1.0 of theoretical. (A third densification stage is possible; however, since the residual porosity containing entrapped gases from the decomposition of Si$_3$N$_4$ is so low, the pressure of the entrapped gas prevents complete densification.) Increasing the temperature (at constant pressure) of hot-pressing increased the rate of densification by at least a factor of 10 between 1650" and 1750"C. Bowen et al. [32] states that the mechanisms causing deformation of the particles include: lattice diffusion (Nabarro-Herring creep), grain boundary diffusion (Coble creep), and liquid-phase solution-precipitation sintering. The rate of densification is also proportional to the amount of grain boundary phase (hence MgO content); the rate-limiting step is the reaction at the phase boundary leading to dissolution at the particle contact points.

The phase transformation was observed during this second stage, with complete conversion at 1750"C in 30 min. From a plot of the % α remaining versus time, the transformation was determined to be first order. The applied pressure causes the α phase to go into solution and reprecipitate as the β phase.

Results of this work showed that both densification and phase transformation are controlled by the same species diffusing in the same direction. Both factors had the same rate dependence on the temperature and additive concentration; however, the transformation rate was pressure independent.

2.4.2 Hot-Pressing Additives

Initial hot-pressing of Si$_3$N$_4$ involved the additive MgO, but the degradation of the high temperature properties due to the low melting magnesium silicate grain boundary phase resulted in the search for more refractory glass and/or crystallized grain boundary phases. Gazza [33] (1973) first added Y$_2$O$_3$ to produce a more refractory reaction product. Full density was obtained with between 5 - 20 wt% Y$_2$O$_3$ in Si$_3$N$_4$ powders with varying purity (the absence of Ca, Na, Fe, and other metals also increased the refractoriness of the second phase); SiO$_2$ was present as an amorphous oxide film on the surface of the Si$_3$N$_4$ particles. X-ray diffraction has shown the major grain boundary phase to be yttrium orthosilicate, Y$_{4.67}$(SiO$_4$)$_3$O, and a small amount of Y$_2$Si$_3$O$_3$N$_4$, an oxynitride [34]. The resulting high temperature (1300"C) strengths were almost double those of fully dense HPSN with MgO and do not decrease until above 1400"C. The oxidation resistance around 1000"C, however, was lower than that for the MgO samples.

Al$_2$O$_3$ has been added to the Si$_3$N$_4$+Y$_2$O$_3$ at the 3 wt% level to lower the liquid formation temperature; this additive in the silicate liquid phase hinders crystallization to promote a glassy grain

boundary. The Al_2O_3 provides good oxidation resistance at 1000"C and has the same strength as the Al_2O_3-free $Si_3N_4 + Y_2O_3$ up to 1200"C (where the $Si_3N_4 + Y_2O_3 + Al_2O_3$ begins to soften, allowing shear between the Si_3N_4 grains). The grain boundary phase in these samples was X-ray diffraction amorphous [34].

The ideal hot-pressing additive(s) for Si_3N_4 would form a liquid phase at hot-pressing temperatures and pressures, allowing full density to be achieved through liquid-phase sintering; only a crystalline phase would remain after this process. Desirable characteristics of the crystalline phase would include [35]:

1. Crystallization from a glassy phase that allows complete densification via liquid phase sintering,

2. Crystallization from a glassy phase without a large change in volume to prevent the formation of residual stresses. detrimental to the final strength,

3. A thermal expansion close to that of β-Si_3N_4 ($\approx 3.2x10^{-6}$/"C). and

4. Good mechanical strength properties so that the strength of the grain boundary is enhanced by crystallization.

Research by Soviet scientists has shown the existence of a crystallized phase being formed from a Y-Si-Al-O-N combination. known as Y-SiAlON [6.7]. This composition is formed from combinations of Y_2O_3, Si_3N_4, SiO_2, Al_2O_3, and AlN. Liquid phase from this additive composition was produced in the region of 1750"C. Studies on the properties of these Y-SiAlONs have shown them to have higher density. glass transition temperature, thermal diffusivity. elastic modulus. hardness, and fracture toughness than corresponding oxide glasses [36,37,38,39]. Since nitrogen is trivalent. it can link to three silicons compared to only two for oxygen. This increases the network-forming (cross-linking) in the structure, producing a tighter, stronger structure. Al_2O_3 increases the nitride solubility in the system; the properties listed above improve with increasing nitrogen content. Toughness. for example. increased by one-third over the nitrogen-free material.

2.5 Fiber Composites

Inclusion of fibers in a ceramic material have been shown to increase the fracture toughness (K_c) of the ceramic matrix composite (CMC) over that of the monolithic body. The composite provides sources of energy adsorption to reduce or prohibit crack propagation not found in a monolithic material.

2.5.1 Toughening Mechanisms

Brennan [40] stated that in fiber composites there are five energy absorbing mechanisms that may be operative: (1) fiber pullout, (2) fiber fracture, (3) delamination. (4) interfacial splitting, and

(5) ductile fiber fracture. Items 4 and 5 have been found to be important in maximizing energy adsorption and controlling the type of fracture in ceramic systems. Interfacial splitting may occur in CMC that have a relatively weak fiber-matrix interface (approximately one-fifth the strength of the fiber); this mechanism blunts propagating matrix cracks and may cause shattering of the matrix. Ductile fiber fracture may occur in composites that contain extremely ductile fibers which allow energy absorption due to local extensive deformation of the fibers at the fracture surface. The goal is to design for controlled failure of the CMC rather than complete catastrophic fracture.

An important contributor to toughness is the load transfer from the matrix to the fibers, resulting from the fibers having a higher Young's modulus than the matrix (at least a 2:1 ratio) [41]. Considerable microcracking of the matrix can be tolerated since the fiber reinforcement will aid in arresting crack growth in the stress field. Matrix microcracking is useful when strong fibers are placed in a weak matrix material with a strong interfacial bond; this mechanism also occurs when the thermal expansion of the the matrix is slightly higher than that of the fibers. Residual stresses result when the matrix is placed in tension upon cooling from fabrication temperature. Crack deflection may be obtained through the mechanism of fiber debonding in the stress field, resulting in energy dissipation without directly contributing to crack extension. Debonding at the fiber-matrix interface occurs in CMC where the fiber and matrix are relatively strong but the interface is weak.

In a recent article Rice [42] states that "it is generally accepted that good toughness results in these composites only when there is limited bonding between the fiber and matrix." This means that mechanical rather than chemical bonding is important and allows for slight bending or twisting of the fibers and good conformity of the matrix to the fibers. Fiber pullout results when a CMC of this type fractures. The mechanical performance of the CMC is determined by the fiber-matrix interfacial shear resistance. Work involving the reaction of carbon fibers with a CVD applied matrix coating of β-SiC showed that tensile strength decreased by about 50% when a 0.6μ reaction layer had formed between the fiber and SiC matrix [43].

Conversely, toughness may increase with extensive fiber-matrix bonding. Compatibility between the matrix and reinforcement must result in sufficient interfacial bonding to yield good mechanical properties (adequate stress transfer at the interface). In general, extensive degradation of the fiber by reaction and interdiffusion must be avoided. Densification aids may be the controlling factor in this degradation. A recent study by Michalske [44] explains how even strongly-bonded fibers can slightly increase toughness by influencing crack propagation.

2.5.2   SiC Fibers

There is major potential for the use of continuous SiC fibers in CMC due to their strength, stiffness, and high temperature stability. The incorporation of the fiber in a ceramic matrix would not only increase the strength but also increase the toughness of the material. Present research efforts have

13

been aimed at minimizing the disintegration of the fibers by the sintering additives and/or matrix at the temperatures necessary to achieve nearly dense ceramics.

Chemical vapor deposition (CVD) of SiC onto a carbon monofilament substrate is the process used to produce continuous SiC fiber[1]. Figure 11 gives a schematic representation of the cross-sectional composition of the SCS-6 fibers. The fiber is 142 μ in diameter with a 33 μ carbon core. A thin coating of pyrolytic graphite (1-1.2 μ) is first deposited on the carbon substrate. The chemical decomposition of a silane-hydrogen gas mixture then causes deposition onto the resistivity-heated, graphite-coated filament as it passes through a CVD reactor [41]. The deposited graphite is mainly β-phase, exhibiting a columnar structure extending radially from the substrate. The mid-radius boundary shown in Figure 11 is due to the two-stage deposition process resulting from differences in temperature and concentration of the reactant gases. The SCS-6 fiber has a 3 μ thick, carbon-rich outer coating to protect the fibers from damage during production and handling. In addition, this coating controls the interfacial reactions between the fibers and the matrix into which it is being incorporated [41].

An average tensile strength of 4 GPa and a Young's modulus of 400 GPa have been reported for the fibers. These fibers are known to undergo significant strength degradation when exposed to temperatures above 1000°C (outside a matrix). Reactive atmospheres may also affect fiber integrity.

2.6   Mechanical Properties by Indentation

Hardness and toughness are used to describe materials according to their characteristic deformation and fracture processes. An indentation pattern can provide simultaneous data on the deformation and fracture properties for a given solid. Research in the past ten years has developed this concept based on Griffith-Irwin fracture mechanics. The scale of the residual impression is determined by the hardness (H), which quantifies the resistance to deformation, while the scale of cracking is determined by the toughness (K_c), which quantifies the resistance to fracture. The onset of cracking occurs at a critical deformation zone size determined by both H and K_c (and the deformation-controlled indentation field). Deformation is dominant at low indenter loads while fracture dominates at high loads [45]. The stress field is elastic/plastic: the elastic (reversible) component is compressive at the surface, while the plastic (irreversible) component is tensile. The radial cracks produced grow to their final length during removal of the load, the main driving force for this crack growth being the residual stress fields in the material.

---

[1] Avco SpecialityMaterials Division, Lowell, MA

14

2.6.1 Equations

Evans and Charles [46] have developed and tested the equations for H and K_c for ceramic materials using the Vickers indentation test. Dimensional fracture mechanics procedures for obtaining the fracture extension from the stress field gives the following general relation:

$$K_c \Phi / H \sqrt{a} = F_1(C/a) F_2(H/E\Phi) \qquad (2.5)$$

where Φ is a constraint factor, a is one-half the diagonal impression, C is the indentation crack length, E is Young's modulus, and F_1 and F_2 are power functions of the associated variables. The slope of the curve of the above expression divided by F_1 was almost exactly $-3/2$; this same slope was obtained for a penny-shaped crack wedged by a force, P, at its center

$$K = P/(\pi C)^{3/2} \qquad (2.6)$$

The equation for Vickers hardness is

$$H = 0.47 P/a^2 \qquad (2.7)$$

By determining the component of P normal to the surface in a Vickers test (neglecting friction), and substituting for P, a relation for K_c is obtained:

$$K_c \Phi / H \sqrt{a} = 0.15 k (C/a)^{-3/2} \qquad (2.8)$$

where $k = 3.2$ (a correction for the presence of the free surface) and $\Phi = 3$ [46].

This technique correlates well with the wedged-crack technique for measuring K_c by fracture analysis methods. K_c measurements have been shown to be accurate within 10% if E is known or within 30% if E is unknown. Values of H and K_c obtained for Si_3N_4 by several techniques are found in Appendix A [47,48,49,50,45,51,52].

2.6.2 Vickers Technique

A Vickers diamond is lowered onto the material surface and the load is applied through the indenter for a set time. Upon removal from the surface the indentation is examined and measured using an optical microscope. The length of the diagonals (a) and cracks (C) produced are measured for use in the H and K_c equations.

This technique requires a small area of sample. The specimen need not be extremely flat, although it needs to be polished in order to clearly see the indentation and cracks. In addition, indentation may not be suitable for coarse-grained or porous ceramic materials. Indentation loads should be high enough so that $C \gg a$, but low enough so that no chipping occurs from lateral cracks reaching the surface (producing material erosion).

Chapter 3

Experimental Procedures

3.1   Matrix 1: HIP'd Reaction-Bonded Si_3N_4

The focus of work at NASA-Lewis was the formation of a matrix material based upon reaction-bonding and densifying Si_3N_4. Two different concentrations of the sintering composition were added to the matrix. The different concentrations yielded 8.0 wt% Y_2O_3 and 3.2 wt% Y_2O_3 (respectively) in the final piece. This additive had the following elemental composition: 25.2 wt% Y, 21.5 wt% Si, 11.6 wt% Al, and 41.7 wt% O. (this sintering additive will be referred to as 'NASA'). It was chosen because the Al_2O_3-Y_2O_3-SiO_2 phase diagram (Figure 12) showed that it would form a liquid phase around 1450"C [53]. Nickel oxide (NiO) was the nitriding aid for each composition above, added at the 2.5 wt% level. The silicon metal powder was a high purity, low oxygen content material[1], while the additives were all commercially available, reagent grade chemicals. All the compositions were prepared by attrition milling in heptane for 24 hr in a Si_3N_4 container with Si_3N_4 media. This procedure broke up agglomerates and decreased the maximum particle size to less than 5 μ (observed by scanning electron microscopy). Each composition was allowed to dry overnight before the next phase in the process.

The sample test bars for subsequent nitridation and sintering were prepared by dry pressing and isostatic pressing. Each bar was prepared from approximately 2.6 g of powder and eight 2.5-3.0 mm long sections of AVCO SCS-6 SiC fibers[§] (approx. 0.15 mm in diameter). The stainless steel die was 34.0 mm long by 7.25 mm wide; the use of 2.6 g of powder produced a test bar having dimensions of 34.0 by 7.25 by 7.25 mm. Samples were pressed in an hydraulic Carver Press at 20.7 MPa (3000 psi). Each sample was then placed in an elastic tube, evacuated, and sealed for isopressing to 413 MPa (60000 psi). No binder was used in the preparation of these test bars. Green densities of the bars from the three compositions ranged from 1.4 - 1.7 g/cc.

---

[1] Superior Graphite Co., Chicago, Il.

Nitridation of the bars was performed in an atmosphere-controlled alumina tube furnace. The bars were placed on Si_3N_4 setters in alumina boats and loaded into the tube. The atmosphere was allowed to flow through the sealed tube for one hour before the nitriding program was started: the exhaust gas was sent through a water bubbler to maintain a high quality nitrogen or hydrogen/nitrogen atmosphere throughout the entire run. The firing schedule was: $10°C/min$ to $1200°C$; 40 hr hold; $10°C/min$ cool. Gas flow rate for the nitriding atmosphere was approximately 2.3 l/min. Four bars of each composition were nitrided in a 100% nitrogen atmosphere, while four additional bars of each were nitrided in a 4% hydrogen nitrogen (by volume) atmosphere to form reaction-bonded Si_3N_4.

After the nitridation reaction was completed. one bar from each composition and nitriding atmosphere was fractured and polished to observe the matrix and fiber-matrix chemical interaction. The other test bars were sintered in a hot isostatic press (HIP) at 5.1 MPa (50 atm) nitrogen overpressure at various temperatures. Nitrided samples were sintered at 1350, 1400 and $1450°C$; and the resulting densities measured. Optical and scanning electron microscopes were used to observe the fractured and polished cross-sections of each densified bar.

3.2   Matrix 2: Pressureless Sintered Reaction-Bonded Si_3N_4

The next stage of research was aimed at densifying RBSN through pressureless sintering in a nitrogen atmosphere. Dry pressed bars were formed containing various levels of Y_2O_3 and constant percentages of NiO and a wax binder.

Batches were mixed based upon a final product of 250 g of RBSN after nitridation. The five compositions contained 0, 2.0, 4.0, 8.0, and 12.0 wt% Y_2O_3. As before. high purity silicon powder was the metal source. One wt% NiO was added to aid nitridation and 1.0 wt% of a polyethylene wax binder was used to provide the test bars with enough green strength for handling. Each of the compositions was ball milled with cylindrical alumina grinding media for 4 hr in heptane. Upon drying, the powders were ready for dry pressing.

The prepared powders were dry pressed[2] at a pressure of 10.3 MPa (1500 psi). The die size was 50 mm long by 10 mm wide: filing the die with 6.0 g of powder resulted in a bar of approximately 7 mm in height. The pressing operation involved filling the die cavity with half of the 6.0 g of powder. laying in 6, 30 - 40 mm sections of SiC fibers. and then burying the fibers with the remainder of the powder. After pressing, the bars were stored in a dry air awaiting nitridation.

The need to nitride these bars resulted in the construction of an atmosphere controlled tube furnace. The furnace is powered by eight spiral SiC heating elements to produce a maximum internal temperature of over $1500°C$ (at the center of the alumina tube). A programmable digital

---

[2] Denison Multipress

17

controller[3] was chosen to control the furnace, allowing gas atmospheres to be automatically altered at different steps in the programs (up to 16 program steps). Gas flow regulation and shutdown, over-temperature protection, cooling system interruption, and audible alarms were also provided. Exhaust gases were sent through a water bubbler.

All of the samples were fired in an atmosphere of prepurified nitrogen (99.998% min. purity, $O_2 \leq$ 5ppm, $H_2O \leq$ 3ppm), flowing through the tube at 2.0 l/min. The firing schedule for each set was: 10"C/min to 300"C; 300"C for 1 hr; 20"C/min to 1300"C; 1300"C for 24 hr; 20"C/min cool. The pressed bars were placed on Si_3N_4 setters in Al_2O_3 boats and loaded into the 250 mm hot zone of the tube. The tube was evacuated and then backfilled with nitrogen three times before the program was started. The lower initial ramp rate and one hour dwell at 300"C allowed for wax burnout. Upon cooling, one bar from each of the five compositions was retained for characterization.

The next step was to pressureless sinter the bars at various temperatures. A Centorr M60[4] vacuum/atmosphere-controlled furnace was utilized for the sintering runs. The furnace, heated with tungsten mesh metal elements, was evacuated three times and backfilled with prepurified nitrogen: the furnace was allowed to pressurize to approximately 0.2 MPa. One of the nitrided bars from each composition was placed on Si_3N_4 setters on a graphite holder. The furnace was heated to the final sintering temperature at a rate of 30"C/min and held for six hours. The bars were sintered at five different temperatures: 1550, 1600, 1650, 1700, and 1750"C.

Densities were measured for all of the bars from this series of experiments. Bars were fractured to look at the fracture surfaces and determine the degree of fiber-matrix interaction and possible strength-controlling mechanisms (due to the fibers). Photomicrographs were taken of the matrices and of fiber-matrix interactions.

3.3   Matrix 3: Hot-Pressing of Various Si_3N_4 Powders

Up to this point in the research on composites for NASA the starting materials had been based on silicon. The most recent work was then directed toward densifying Si_3N_4 powder by hot pressing as the matrix material. The triple oxide combination (Y_2O_3-Al_2O_3-SiO_2) used in the hot isostatic pressing of RBSN (Matrix 1) at NASA was compared with a oxide-nitride composition reported by a group of Soviet scientists [6,7]. Four different Si_3N_4 powders with five weight percent of the two different sintering additives were compared; SiC fibers were placed in two of the best powders in a final hot press run to determine the degree of interaction between the matrices and fibers and the effect of fibers on the densification of the hot-pressed Si_3N_4 matrix.

---

[3] Eurotherm 821 Programmable Controller, Eurotherm Corp. Reston, MD.

[4] Centorr Associates, Suncook, NH

The triple oxide composition ultilized was the NASA composition from Matrix 1. This batch was milled for 24 hr in distilled water with Si_3N_4 media and then dried at 60"C. Agglomerates were broken up in a mortar and pestle.

The oxide-nitride sintering aid was similar to the triple oxide aid. the major difference being the replacement of Al_2O_3 with AlN. The elemental weight percent of the additives were 60.7 wt% Y, 7.7 wt% Si, 5.5 wt% Al, 18.6 wt% O, and 6.7 wt% N. (This composition will be referred to as 'Y-SiAlON'.) The additive was prepared from SiO_2 (added as a colloidal suspension. Ludox AS-40), Y_2O_3, and AlN powder. The batch was ball milled for 24 hr in heptane with Si_3N_4 media and dried. The additive was then ball milled dry with Si_3N_4 media to break up the dried agglomerates.

All of the hot-pressed pieces were made from different Si_3N_4 powders with five weight percent of the sintering additives. The four powders were: (1) Starck H1[5], (2) Ube SN-E-10[6], and KemaNord[7] (3) P95 and (4) S95. Appendix B contains data on the characteristics of each powder, including surface area, oxygen, and metal impurity contents. The powders were ball milled in heptane for 12 hr with the same spherical Si_3N_4 grinding media as before. After drying the soft agglomerates were reduced in a mortar and pestle. ready for hot pressing.

The hot press was a rf induction. graphite-based unit[5], able to achieve more than 2200"C and apply a pressure of 34.5 MPa (5000 psi) on a 150 mm (6 in) diameter ram. The mold was made from a 200 mm diameter cylinder of electronic-grade graphite. 300 mm in height. Four 50 mm holes were bored parallel to the center; graphite rams and spacers were milled to fit each hole, allowing for a non-interference fit between the die parts. This mold design allowed for 12 discs to be made in each hot pressing cycle. three in each column. Pressure was applied through a hydraulic cylinder after the temperature had surpassed 1000"C. A preliminary run was made using Y-SiAlON in the Ube and Starck powders. The temperature reached 1775"C at 34.5 MPa during the 1 hr dwell.

In the second run all four Si_3N_4 powders containing the NASA aid were hot-pressed. Grafoil (graphite tape) was placed between the powder samples and the spacers and rams to reduce the reaction of the mold with the powder; 25.0 g of sample were used to make each disc. The maximum temperature during the run was 1775"C. but the pressure only went to 24.8 MPa (3600 psi) to prevent mold failure during the run due to a shift in the alignment of the carbon and graphite mold stack. The temperature and pressure were held for 1 hr. Upon cooling, the densified discs were forced out of the graphite mold. The grafoil was removed from the surfaces by manually grinding the discs on a 165 μ metal-bonded diamond disc.

In the third hot press run the Starck and both KemaNord powders were densified containing 5 wt% of the Y-SiAlON additive. Each disc was made from 20.0 g of each powder; four of each

[5] Hermann C. Starck Berlin, W. Germany

[6] Ube Industries Ltd., Tokyo, Japan

[7] KemaNord Industrikemi, Nobel Industrier, Ljungaverk, Sweden

[8] Alfred Ceramic Enterprises, Alfred Station, NY

was prepared. The pressure reached 34.5 MPa and the temperature reached a maximum of 1760"C during the 1 hr hold. The discs were removed and polished as before.

The fourth run involved only the KemaNord P95 and S95 Si_3N_4 powders but with a new addition. Two discs of each were prepared from 20.0 g of the powders containing the Y-SiAlON aid; these were present as a control group to compare with the results from run 3. Four discs of each powder were also made containing eight 20 - 30 μ sections of SiC fiber used in the previous matrices. These samples were prepared by placing approximately half of the powder in the mold. leveling the powder surface, laying the fibers on this surface. and then burying them with the remainder of the powder. The sample preparation was the same as in run 3, as were the temperature and applied pressure.

All of the hot-pressed samples were checked for densification by use of the Archemedes Balance Technique (ASTM C373-72(82). The microstructure and the fiber-matrix interaction were examined by optical and scanning electron microscopy. Two important mechanical properties were also tested in these specimens.

3.4   Hardness and Toughness Measurements

Hardness and toughness values for all of the various matrices were determined by indentation analysis utilizing a Vickers diamond. The hot-pressed and HIP'd RBSN samples were tested on a Buehler Micromet II Microhardness Tester, applying a 1 kg load. Due to the porosity of the pressureless sintered RBSN matrices. higher loads were needed to make an indentation that could be measured; these samples were indented on an older Tukon Tester which could apply a 3 kg load. Constant indentation time for all of the samples was 15 sec. Measurements of both the diagonal lengths and the crack lengths were made on the Buehler unit. which had a microscope with 1000x magnification and a filar eyepiece.

Chapter 4

Results and Discussion

4.1 Matrix 1

The density data for the HIP'd SRBSN samples was observed to be independent of that of the nitriding gas after sintering. The nitrided bars with high Y_2O_3 content (8.0 wt%) were less than 10% denser than the nitrided bars with low Y_2O_3 content (3.2 wt%)(1.61 g/cc compared to 1.48 g/cc for the N_2 atmosphere bars, and 2.43 g/cc versus 2.34 g/cc for the H_2/N_2 atmosphere samples). Nitriding in the presence of 4 vol% H_2 made a major difference in the nitrided densities; the high and low additive RBSN samples were much denser than those same compositions nitrided in a nitrogen-only atmosphere (2.48 and 2.35 g/cc compared to 2.49 and 2.35 g cc. respectively). The density differences were insignificant after overpressure sintering, however. The density of all overpressure-sintered bars fell within ± 0.10 g/cc of 2.42 g/cc. Temperature did not affect the resulting sintered densities.

Hardness and toughnness values for the Matrix 1 samples are found in Appendix C. For the high additive bars nitrided only in nitrogen, hardness and K_c were half that of the same HIP'd bars. The low additive nitrided and HIP'd bars had the same values for these mechanical properties even though the HIP'd samples were denser. Examination of the bars (both high and low Y_2O_3) nitrided in the mixed gas atmosphere showed that the nitrided bars had the same hardnesses and toughnesses as those bars HIP'd at the various temperatures; sintering temperature appeared to have no effect on these values. The hardness values were the same for the high and low Y_2O_3 samples.

Representative microstructures of the samples are shown in the next series of micrographs. As shown in Figure 13, the nitrided microstructure of the samples from the H_2/N_2 atmosphere is more uniform and less porous than the samples from the N_2 atmosphere. Figure 14 exhibits the lack of interaction between the fiber and matrix.

Figure 15 represents the lack of fiber/matrix interaction occurring in all of the HIP'd samples

based upon the Y_2O_3-Al_2O_3-SiO_2 additive composition. Very slight degradation of the outer carbon layer has been produced at either additive level, and sintering temperature does not seem to have affected this layer either. This is in sharp contrast to the same fibers in a SRBSN matrix with 6.0 wt% MgO, shown in Figure 16. This sample, produced for comparison to this study by the same experimental methods exhibits serious chemical reaction of the matrix and SiC layer.

Figure 17 compares the high additive matrix HIP'd at 1400 and 1450°C. There is little difference between the two microstructures; the same is true for the low additive SRBSN samples. At these temperatures only first stage sintering seems to have occurred. A large degree of inhomogeneity is present over the cross-section of a RBSN sample, exhibited clearly by the two micrographs on Figure 18.

4.2   Matrix 2

As shown in the Figure 19, the density of the nitrided bars increased with increasing Y_2O_3 content. The 0 and 2.0 wt% Y_2O_3 bars had the same densities, while those with 4.0, 8.0, and 12.0 wt% Y_2O_3 samples increased by 4.2, 7.0, and 8.6%, respectively. A representative microstructure is shown in Figure 20.

Sintering greatly increased the density of the nitrided bars containing Y_2O_3, shown in Figure 21. The density of the 2.0 and 4.0 wt% Y_2O_3 bars had densities between 2.1 - 2.2 g/cc; those of the 8.0 and 12.0 wt% bars had densities in the 2.2 - 2.3 g/cc range. Increasing sintering temperature yielded higher densities in the 2.0 and 4.0 wt% than the higher Y_2O_3 samples. The opposite was true at 1550, 1600, and 1650°C. RBSN bars containing no Y_2O_3 showed a decrease in density upon sintering. At the same time these Y_2O_3-free bars appeared to suffer increasing amounts of decomposition as the sintering temperature increased form 1550 to 1750°C.

For the nitrided samples, hardness and toughness increased slightly as the Y_2O_3 content increased. These values for the samples sintered at 1550, 1600, and 1650°C were the same across the additive range. However, at the higher temperatures, the hardness and toughness values varied significantly over the range of additive levels. The Y_2O_3-free samples sintered at 1700 and 1750°C had values similar to the nitrided samples. The values for the 2.0 and 12.0 wt% samples were lower than those with 4.0 and 8.0 wt% Y_2O_3. The highest hardness value for any of the pressureless sintered samples was 0.52 GPa, while the maximum K_c was 0.48 MPa m$^{1/2}$. Appendix D contains the density, hardness, and K_c values for the Matrix 2 samples.

Three characteristic fracture surfaces were observed in these samples (all bars broken in a four-point bend apparatus). The first type exhibited fiber pull-out from the matrix; the carbon core fractured at the level of the fracture surface, while the SiC and outer carbon layer fractured and pulled away from the matrix. The central carbon core appears to have blunted the crack that

travelled through the bulk of the fiber. This behavior, shown in Figure 21, occurred predominantly in the unsintered, nitrided samples due to no apparent chemical bonding to the matrix (as observed in the figure). In addition, some of the bars remained in one piece since the fibers did not fail during fracture. (All of the fibers in these samples showed cantilever curl on their fracture surface.)

The samples sintered at low temperatures displayed the second type of fracture surface, where a small amount of fiber pull-out was present both at the carbon core and SiC layer. For the most part the fracture surface appeared relatively flat with a limited amount of fiber/matrix chemical interaction; porosity had become finer and some necking between grains was apparent. Shown in Figure 22, these examples show the degree of interaction (Figure 22b shows that a pore in the central carbon core may have been the source of fracture).

High sintering temperatures produced the third characteristic type of fracture surface. As shown in Figure 23, the fibers in these matrices are tightly bonded to the matrix compared to the previous micrographs (Figures 21 and 22), with pull-out occurring only at the carbon core. The bonding caused the fiber to fail at the level of the fracture surface as if it were part of the matrix. In addition, it is observed that the crack front was blunted when it encountered fibers. Randomly distributed larger grains are becoming apparent at the higher sintering temperatures.

4.3   Matrix 3

The four Si_3N_4 powders used in hot-pressing showed varying degrees of densification. Each powder had differing levels of impurities (ie., oxygen, iron) that could contribute to the property differences. All of the starting powders had surface areas near 10 m^2/g.

The triple oxide sintering additive (Y_2O_3-Al_2O_3-SiO_2) samples had densities that were approximately 0.1 g/cc higher than those hot-pressed with the oxide-nitride composition. The Ube sample had the lowest density (2.87 g/cc) and showed regions of decomposition at the edges of the sample. The KemaNord samples had highest density and hardness values for the hot-pressed samples (both additive compositions), being greater than 3.0 g/cc and 1.69 MPa $m^{1/2}$, respectively. The toughness showed no trend, however; the KemaNord P95 sample had the highest toughness of all the samples produced (1.80 MPa $m^{1/2}$), while the densest, highest hardness KemaNord S95 sample had the lowest hot-pressed toughness (0.80 MPa $m^{1/2}$).

The Y-SiAlON sintering additive produced lower densitites for the same additive level and hot-pressing conditions, and lowered the values of the corresponding mechanical properties. Again, the Starck powder produced hot-pressed samples with the lowest density and hardness while the KemaNord S95 had the highest values. K_c values were reversed compared to the densities, however. Density, hardness, and toughness values are found in Appendix E.

Photomicrographs of both sets of hot-pressed samples show that the sintering additive com-

position did not affect the sintering behavior of the particular powder. The microstructures of the Ube and Starck samples appear to be less homogeneous than those formed from the KemaNord powders. These micrographs are found in Figure 24 and 25.

The variance of the measurements used to calculate the hardness data for the hot-pressed samples help to statistically show the inhomogeneities of the microstructure. The indentations, made randomly across the sample (at least five per sample), produced diagonals with lengths that varied the least in the KemaNord pieces and the greatest in the Starck pieces. The statistical data is also found in Appendix E.

The addition of randomly arranged fibers caused a decrease in density compared to the matrix-only samples by approximately 0.1 g/cc. Figure 26 shows a fiber extending from a fracture surface in a KemaNord P95 sample. At the 5.0 wt% level for the Y-SiAlON additive (hot-pressed at 1750°C) slight chemical interaction between the matrix and outer carbon layer has occurred without damaging the SiC region of the fibers.

Chapter 5

Conclusions

1. The presence of H_2 in the nitriding gas produces a more homogeneous, dense microstructure in the reaction-bonding of silicon metal powder, with improved hardness and K_c over N_2-only reaction-bonded silicon.

2. Hot-isostatic-pressing increased the density and the mechanical properties of samples nitrided in pure N_2; samples nitrided in H_2/N_2 were not improved significantly. Both types of samples had the same final density and properties.

3. First-stage sintering characteristics were observed in all of the HIP'd samples - higher sintering temperatures should be utilized if possible without degradation.

4. The chosen sintering additives for Matrix 1 do not degrade the SiC fibers (compared to MgO).

5. Decomposition of RBSN occurs during pressureless sintering when no sintering additives are present - no liquid phase to inhibit dissociation of the Si_3N_4.

6. Increasing Y_2O_3-content increases the density (nitrided and sintered); increasing sintering temperature also increases the density of the pressureless sintered samples.

7. Pressureless sintered samples with 4.0 and 8.0 wt% Y_2O_3 had the best hardness and K_c values for Matrix 2 samples.

8. The degree of fiber/matrix bonding affects the type of fracture occurring in the sample. No bond produces mechanical pullout of the fiber, while strong chemical bonding causes the propagating crack front to to bow around the fibers; when the carbon core fails, the fiber fractures and the crack is allowed to advance.

9. Hot-pressing of Si_3N_4 produced the highest density, hardness, and toughness values of all the Si_3N_4 matrices tested here.

10. The KemaNord powders show improved densification behavior over the Starck and Ube powders, producing more homogeneous microstructures with higher densities.

11. Fiber/matrix interaction was very slight at the hot-pressing conditions and additive concentrations utilized to make the Matrix 3 samples.

Chapter 6

Recommendation for Future Work

Additional work should pertain to maximizing sintered density of the matrix while maintaining fiber integrity in the composite; increasing the total percentage of additives, changing the additive composition, and increasing the sintering temperature and/or time may lead to these improvements in all of the matrices tested. The KemaNord powders need to be more thoroughly tested to determine the exact reason they show the best hot-pressing behavior.

Although the RBSN samples failed to show acceptable mechanical properties, further investigations should be undertaken to determine the effect of H_2 on nitridation. The denser, more uniform microstructure produced with the mixed nitriding gas might enable a dense sintered piece to be formed; alteration of the sintering aids and of the pressureless sintering technique should be investigated here.

Finally, further work must be performed in modeling, processing, and mechanical testing of composites. Final properties will depend on the bond between the fiber and matrix, fiber packing density, elimination of matrix defects (ie. voids) near the fibers, and how the composite was tested. Many questions must be answered before ceramic fiber composites will see widespread use.

Bibliography

[1] Technical Staff. *Program Summary, Garrett/Ford AGT-101 Advanced Gas Turbine*. Technical Report, Garrett Turbine Engine Company, June 1984.

[2] Bernard North. Ceramic cutting tools. *Carbide and Tool Journal*. 18(5):23–28. 1986.

[3] J.A.Mangels and G.J.Tennenhouse. Densification of reaction-bonded silicon nitride. *Am.Cer.Soc.Bull.*, 59(12):1216–1222, 1980.

[4] J.A.Mangels and G.J.Tennenhouse. Sintering behavior and microstructural development of yttrium-doped reaction-bonded silicon nitride. *Am.Cer.Soc.Bull.*. 60(12):1306–1310, 1981.

[5] J.A.Mangels and G.J.Tennenhouse. *Method of Densifying a Reaction-Bonded Silicon Nitride Article*. U.S.Patent 4285895, Ford Motor Company, Aug. 25 1981.

[6] I.L.Boyarina. A.B.Puchkov, A.M.Gavrish, Z.D.Zhukova, and E.V.Degtvareva. Sialons - new refractory metals. *Ogneupory (trans.)*, 12(12):24–28, 1981.

[7] S.Boskovic, L.J.Gauckler, G.Petzow. and T.Y.Tien. Reaction Sintering Forming β-Si_3N_4 Solid Solutions in the System Si,Al/N,O: I. Sintering of SiO_2-AlN Mixtures. *Pow.Met.Int.*, 9(4):185–189, 1977.

[8] E.T.Turkdogan and P.M.Bills. Silicon nitride: some physico-chemical properties. *J.Appl.Chem.*. 8:296. 1958.

[9] D.Hardie and K.H.Jack. Crystal structures of silicon nitride. *Nature*, 180:322, 1957.

[10] S.Wilde, P.Grieveson, and K.H.Jack. The crystal structures of alpha and beta silicon and germanium nitride. In P.Popper, editor, *Special Ceramics 5*, page 385, 1972.

[11] H.F.Priest, F.C.Burns, G.L.Priest, and E.C.Skaar. Oxygen content of alpha silicon nitride. *J.Am.Cer.Soc. - Discussion*, 56:395, 1973.

[12] K.Kato, Z.Inoue, K.Kijima, I.Kawada, and H.Tandka. Structural approach to the problem of oxygen content in alpha silicon nitride. *J.Am.Cer.Soc.*, 58:90, 1975.

[13] I.Kohatsu and J.W.McCauley. Re-Examination of the Crystal Structure of α-Si$_3$N$_4$. *Mat.Res.Bull.*, 9:917, 1974.

[14] S.R.Axelson. Electronic and Crystal Structures of *alpha-* and *β-* Silicon Nitride. A report written for G.S.Fischman. NYS College of Ceramics, March 1987.

[15] F.L.Riley. Silicon nitridation. In F.L.Riley, editor, *Progress in Nitrogen Ceramics*. pages 121–134, NATO ASI Series, 1981.

[16] A.J.Moulson. Review - reaction-bonded silicon nitride: its formation and properties. *J.Mat.Sci.*, 14:1017–1051, 1979.

[17] M.W.Lindley, D.P.Elias, B.F.Jones, and K.C.Pitman. The Influence of Hydrogen in the Nitriding Gas on the Strength, Structure, and Composition of Reaction-Sintered Silicon Nitride. *J.Mat.Sci.*, 14(1):70–85, 1979.

[18] N.J.Shaw. *Nitridation of Silicon*. Master's thesis, Case Western Reserve University, Oct. 1981. NASA TM-82722.

[19] J.A.Mangels. Fabrication of complex shaped ceramic articles by slip casting and injection molding. In *Progress in Nitrogen Ceramics*, pages 711–716. NATO ASI Series, 1981.

[20] A.Atkinson and A.J.Moulson. Some important variables affecting the course of reaction between silicon powder and nitrogen. In *Science of Ceramics 8*, pages 111–122. British Ceramic Society, 1976.

[21] A.Hendry. Thermodynamics of silicon nitride and oxynitride. In F.L.Riley, editor, *Progress in Nitrogen Ceramics*, pages 183–185. NATO ASI Series, 1977.

[22] H.Y.Lu and F.L.Riley. The analysis of silicon nitridation kinetic data. In *Science of Ceramics 12*, pages 145–150, Ceramurgica s.r.l., 1984.

[23] M.N.Rahaman and A.J.Moulson. The removal of surface silica and its effect on the nitridation of high-purity silicon. *J.Mat.Sci.*, 19(1):189–194, 1984.

[24] B.F.Jones and M.W.Lindley. The influence of hydrogen in the nitriding gas on the strength of reaction-sintered silicon nitride. *J.Mat.Sci.*, 11(10):1969–1971, 1976.

[25] H.Dervisbegovic and F.L.Riley. The role of hydrogen in the nitridation of silicon powder compacts. *J.Mat.Sci.*, 16:1945–1955, 1981.

[26] H.Dervisbegovic and F.L.Riley. The influence of iron and hydrogen in the nitridation of silicon. *J.Mat.Sci.*, 14(5):1265–1268, 1979.

[27] D.R.Messier and P.Wong. Kinetics of Formation and Mechanical Properties of Reaction-Sintered Si_3N_4. In J.J.Burke, A.E.Gorum, and R.N.Katz, editor, *Ceramics for High Performance Applications*, pages 181-193, 1974.

[28] W.Mustel and D.Broussard. Optimization of the silicon nitridation process. In *Science of Ceramics 12*, pages 131-138, Ceramurgica s.r.l., Faenrza, 1984.

[29] J.A.Mangels. Effect of H_2-N_2 Nitriding Atmosphere on the Properties of Reaction-Sintered Si_3N_4. *J.Am.Cer.Soc. - Discussion*, 58(7-8):354-355, 1975.

[30] R.J.Brook. Developments in the sintering of ceramics. In K.J.deVries, editor, *Science of Ceramics 9*, pages 57-66, 1977.

[31] A.Giachello and P.Popper. Post-sintering of reaction-bonded silicon nitride. *Ceramurgia Int.*, 5(3):110-114, 1979.

[32] L.J.Bowen, R.J.Weston, T.G.Carruthers, and R.J.Brook. Hot-pressing and the $\alpha - \beta$ transformation in silicon nitride. *J.Mat.Sci.*, 13:341-350, 1978.

[33] G.E.Gazza. Hot-Pressed Si_3N_4. *J.Am.Cer.Soc.*, 56(12):662, 1973.

[34] J.T.Smith and C.L.Quackenbush. Phase Effects in Si_3N_4 Containing Y_2O_3 and CeO_2: I, Strength. *Am.Cer.Soc.Bull.*, 59(5):529-537, 1980.

[35] J.E.Weston, P.L.Pratt, and B.C.H.Steele. Crystallization of grain boundary phases in hot-pressed silicon nitride materials. *J.Mat.Sci.*, 13:2137-2146, 1978.

[36] R.E.Loehman. Preparation and properties of yttrium-silicon-aluminum oxynitride glasses. *J.Am.Cer.Soc.*, 62(9-10):491-494, 1979.

[37] R.E.Loehman. Oxynitride glasses. *J.Noncryst.Solids*, 42:433-446, 1980.

[38] R.E.Loehman. *Basic Research on Oxynitride Glasses - Final Report*. Technical Report DAAG-29-79-c-007, U.S.Army Research Office, July 1982.

[39] D.N.Coon, J.G.Rapp, R.C.Bradt, and C.G.Patano. Mechanical properties of silicon-oxynitride glasses. *J.Noncryst.Solids*, 56:161-166, 1983.

[40] J.J.Brennan. Increasing the impact strength of si_3n_4 through fiber reinforcement. In P.Popper, editor, *Special Ceramics 6*, pages 123-134, 1975.

[41] R.Wills, M.Pascucci, F.Jelinek. *Ceramic-Ceramic Composites: A State-of-the-Art Report*. Technical Report MCIC-86-51, Metals and Ceramics Information Center, Jan. 1986.

[42] R.W.Rice. Fundamental needs to improve ceramic-fiber composites. *Cer.Eng.Sci.Proc.*, 4(7-8):484-491, 1983.

[43] R.Pampuch, W.Slomka, and J.Chlopek. Determination of the influence of matrix-ceramic fiber reactions on strength of composites. *Ceramics Int.*, 12:9-18, 1986.

[44] T.Michalske. June 1987. Private communication.

[45] B.R.Lawn and B.Marshall D. Hardness. Toughness. and Brittleness: An Indentation Analysis. *J.Am.Cer.Soc.*, 62(7-8):347-350, 1979.

[46] A.G.Evans and E.A.Charles. Fracture toughness determinations by indentation. *J.Am.Cer.Soc. - Discussion*, 59(7-8):371-372, 1976.

[47] J.A.Smith and Jr. J.L.Shannon. Fracture Toughness of Si_3N_4 with Short Bar Chevron-Notched Specimens. *J.Mat.Sci.*, 22:321-324, 1987.

[48] S.C.Danforth and M.H.Richman. Strength and Fracture Toughness of Reaction-Bonded Si_3N_4. *Am.Cer.Soc.Bull.*, 62(4):501-504, 1983.

[49] Jurgen Heinrich and D.Munz. Strength of reaction-bonded silicon nitride with artificial pores. *Am.Cer.Soc.Bull.*, 59(12):1221-1222, 1980.

[50] J.L.Henshall, D.J.Rowcliffe, and J.W.Edington. The fracture toughness and delayed fracture of hot-pressed silicon nitride. In P.Popper, editor. *Special Ceramics 6*, pages 185-198, 1975.

[51] C.Greskovich and G.E.Gazza. Hardness of Dense α- and β- Si_3N_4 Ceramics. *J.Mat.Sci.Lett.*, 4:195-196, 1985.

[52] S.G.Seshadri, M.Srinivasan, and L.King. Indentation fracture testing of ceramics. *Cer.Eng.Sci.Proc.*, 4(9-10):853-863, 1983.

[53] A.Bondar and F.Ya.Galakhov. Fig. 2586 - System Al_2O_3-Y_2O_3-SiO_2. Phase Diagrams for Ceramists, 1968.
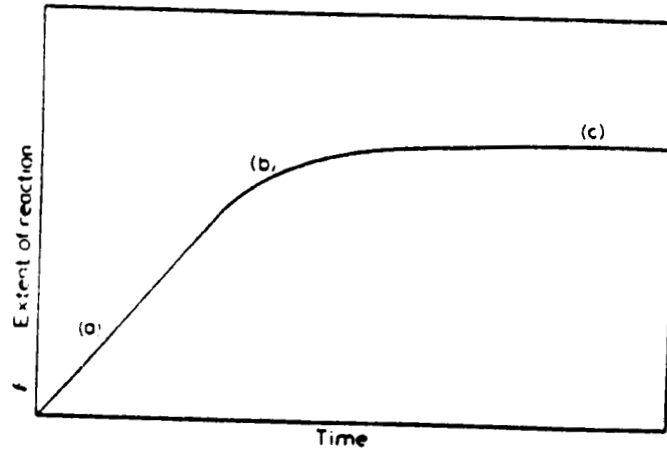
Figure 1: Schematic of reaction kinetics showing the three regions: (a) linear kinetics, (b) decreasing reaction rate, (c) effectively "zero" reaction rate, even though compact is only partially nitrided. [16]
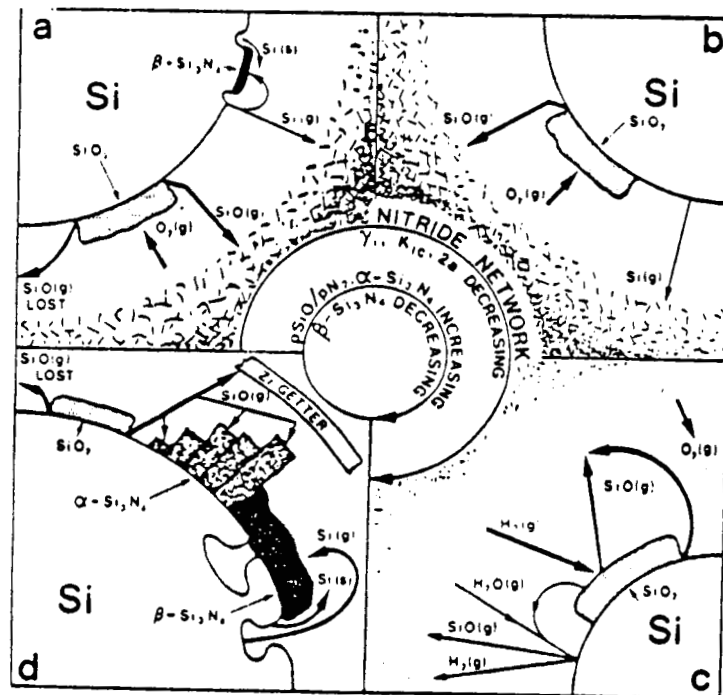
Figure 2: A schematic representation of the influence of the nitriding environment on the mechanism of formation of microstructure, composition, and fracture properties of RBSN. (The reactions, shown with heavy lines, are considered important in determining microstructure and mechanical properties.) [17]
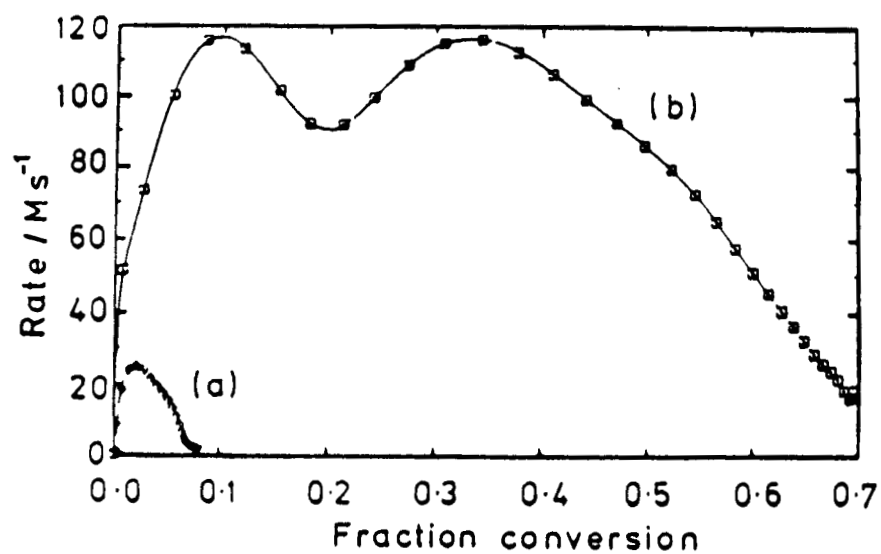
Figure 3: Silicon nitridation under (a) 53 kPa, N_2, (b) 53 kPa, 5% H_2/N_2. Nitridation rates as a function of fraction converted. [22]
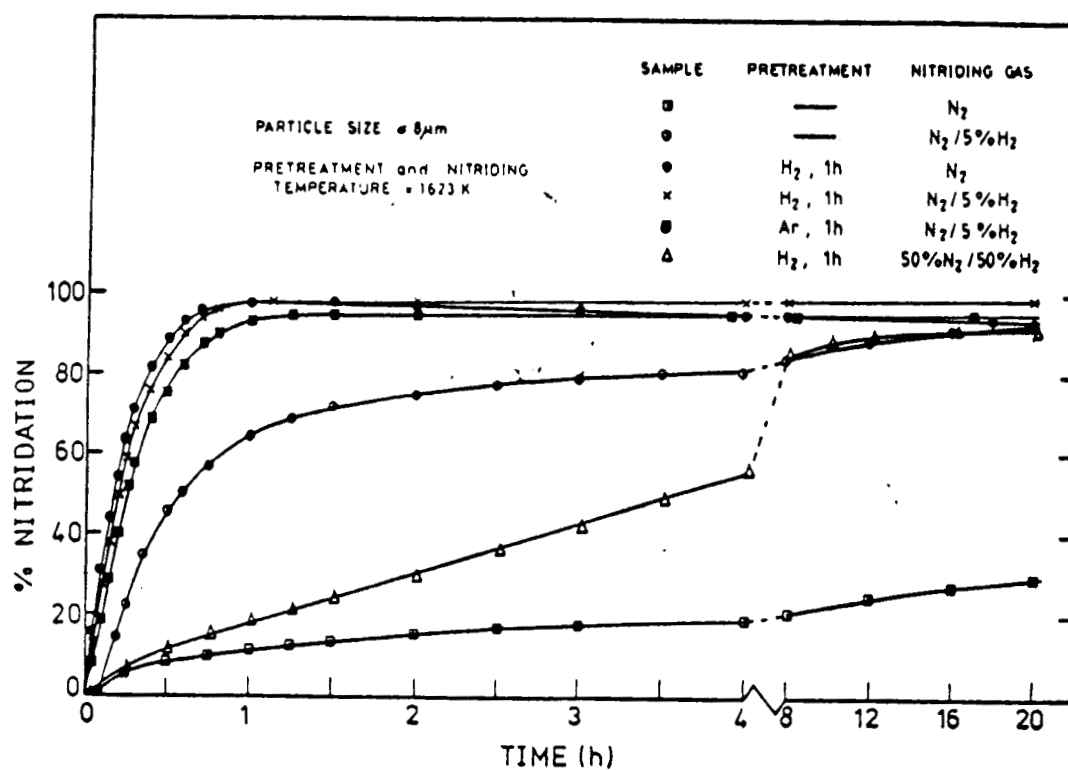
Figure 4: Percentage nitridation plotted against time for samples nitrided following pretreatment in H_2 or Ar for 1 hr and for samples nitrided without pretreatment. [23]
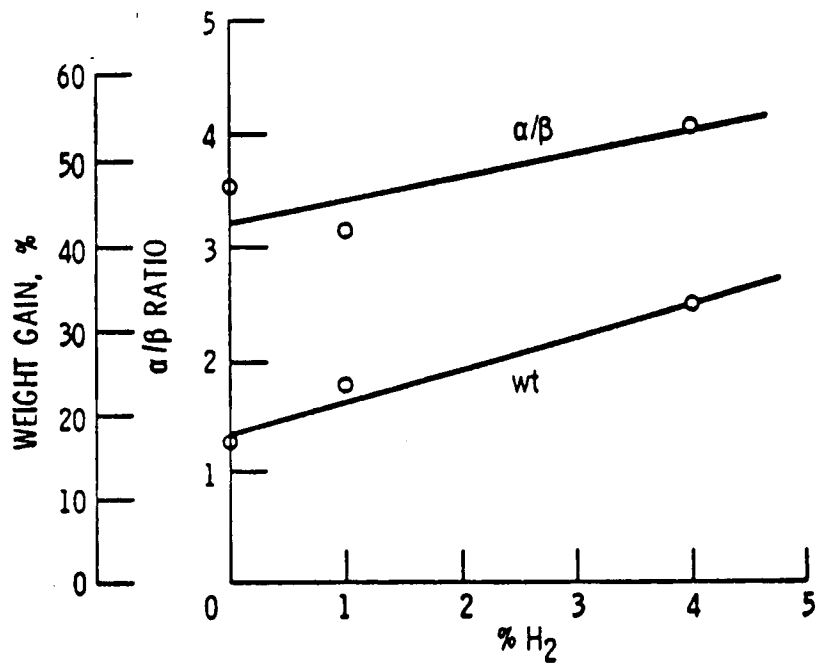
Figure 5: α/β ratio and weight gain of nitrided lower purity Si powder as a function of H_2 content of the nitriding gas (4 hr, 1200"C). [18]
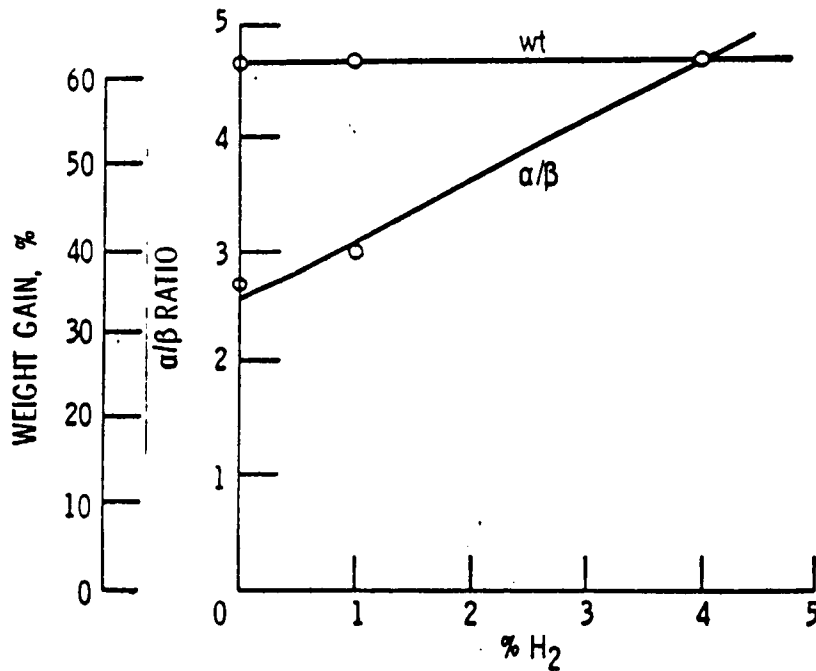
Figure 6: α/β ratio and weight gain of nitrided lower purity Si powder as a function of H_2 content of the nitriding gas (4 hr, 1375"C). [18]
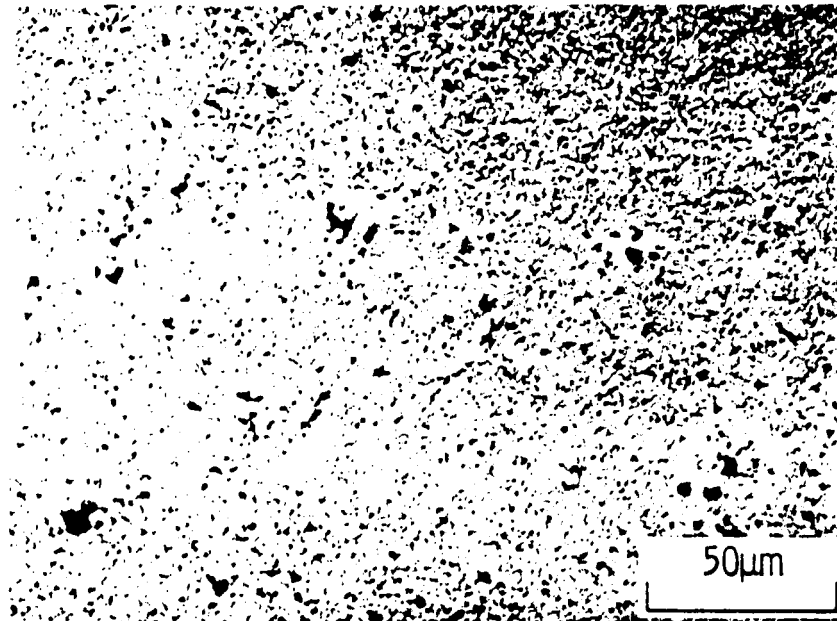
a. Heated in 4% H_2/N_2
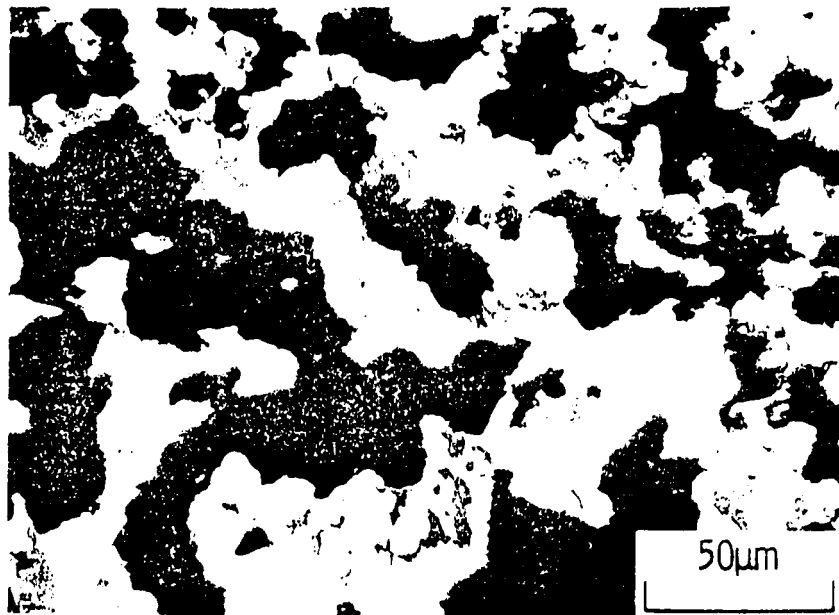
b. Heated in He

Figure 7: Micrograph of polished section of Si_3N_4 from lower purity Si compact nitrided in 4% H_2/N_2 (4 hr, 1375°C). [18]
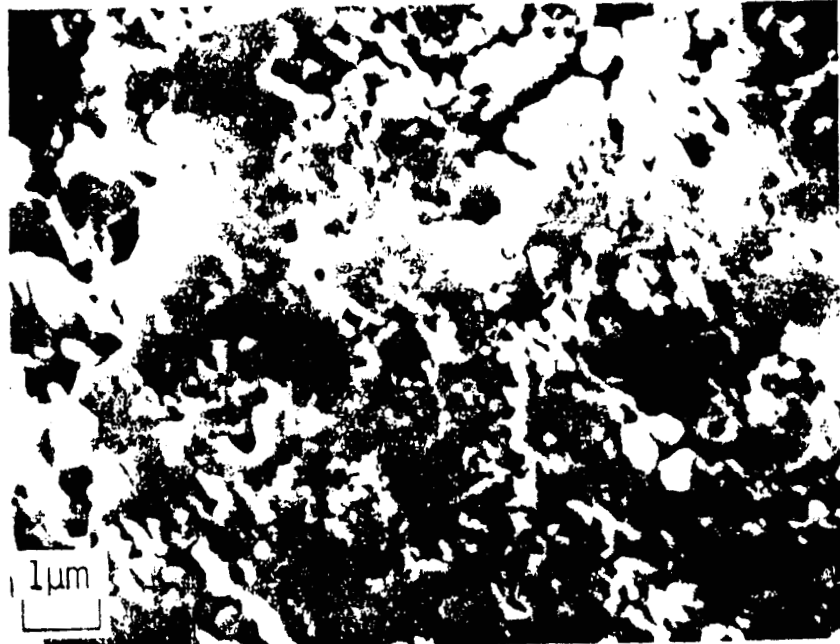
a. in N_2
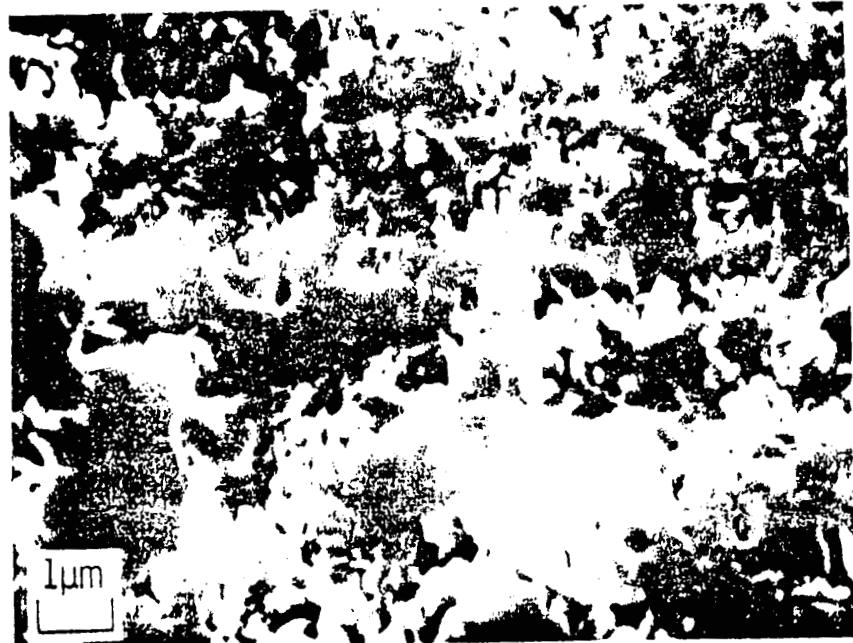
b. in 1% H_2/N_2

Figure 8: SEM micrographs of fracture surface of Si_3N_4 from lower purity Si compact (4 hr, 1375°C). [18]
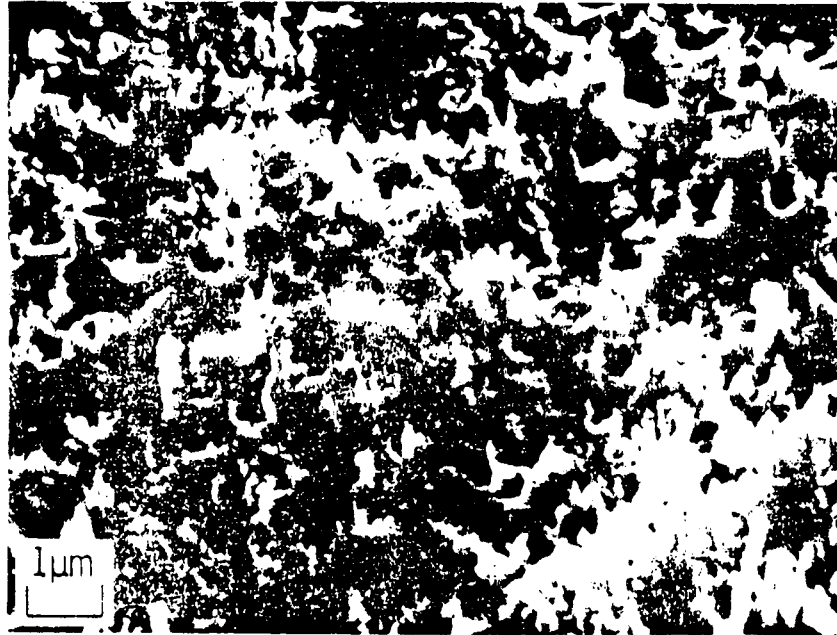
c. in 4% H_2/N_2

Figure 8: SEM micrographs of fracture surface of Si_3N_4 from lower purity Si compact (4 hr, 1375"C). [18]
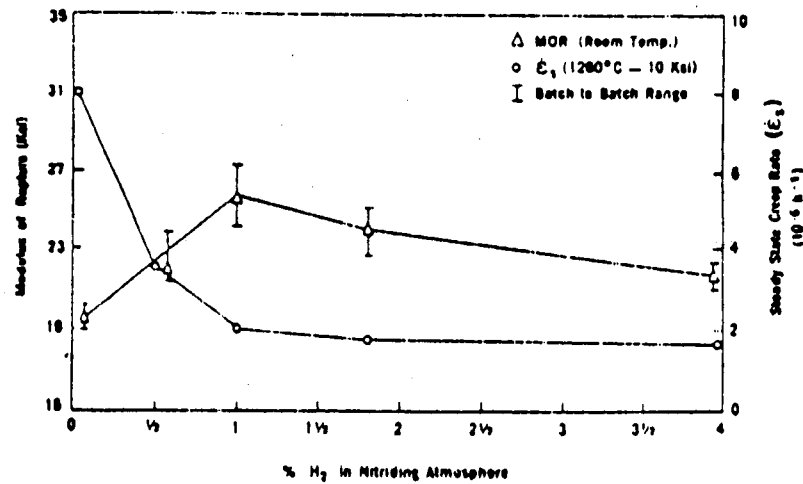
Figure 9: Modulus of rupture and steady-state creep rate as a function of amount of H_2 in the nitriding atmosphere. [16]
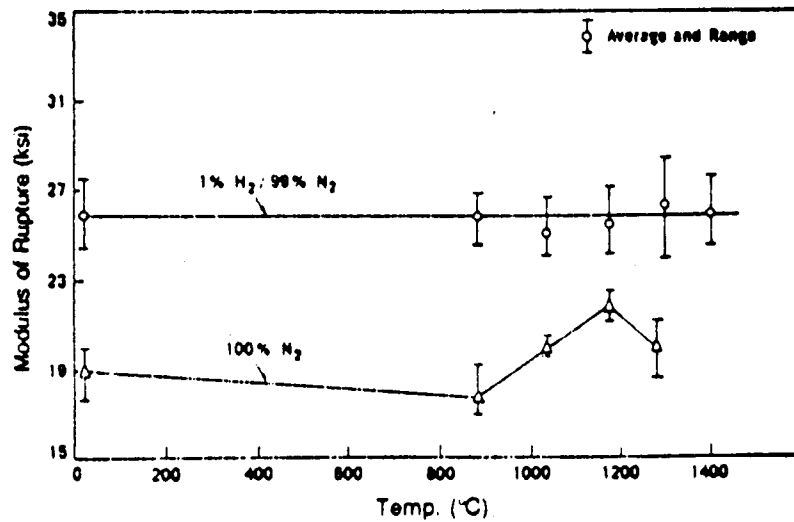
Figure 10: High-temperature modulus of rupture of Si_3N_4 for two nitriding atmospheres.[16]
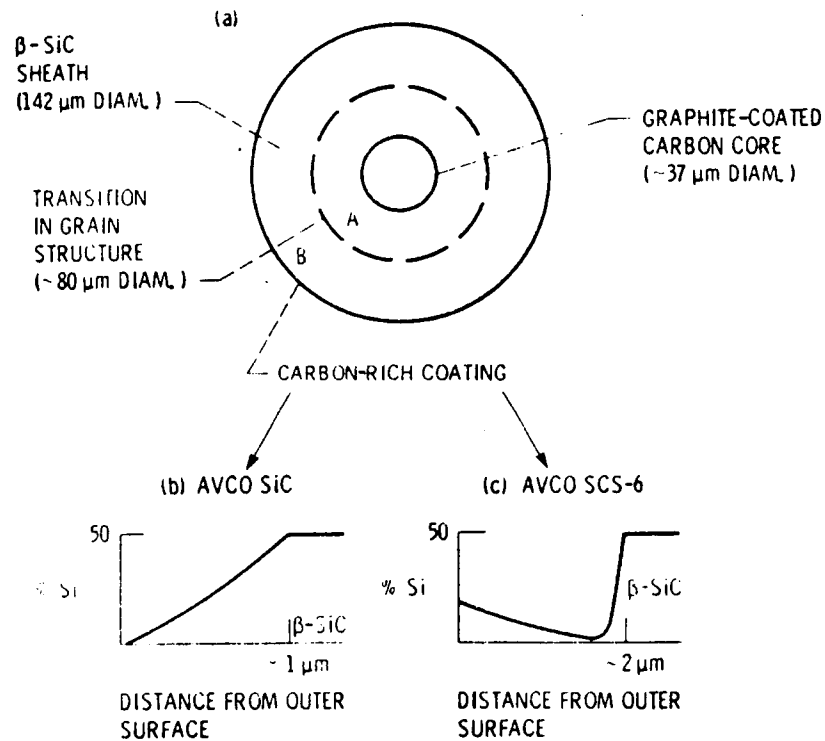
Figure 11: Schematic representations of (a) the CVD SiC fiber cross-section, and (b,c) the silicon content in the two types of carbon-rich fiber coatings. (Courtesy of NASA-Lewis Research Center.)
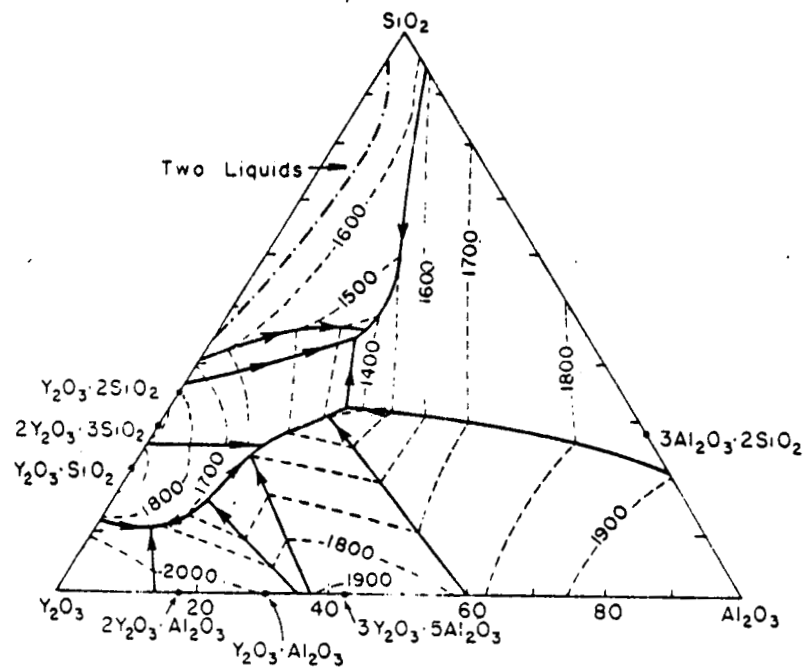
FIG. 2586.—System Al₂O₃-Y₂O₃-SiO₂.

Figure 12: Phase diagram for the Al_2O_3-Y_2O_3-SiO_2 system. [53]
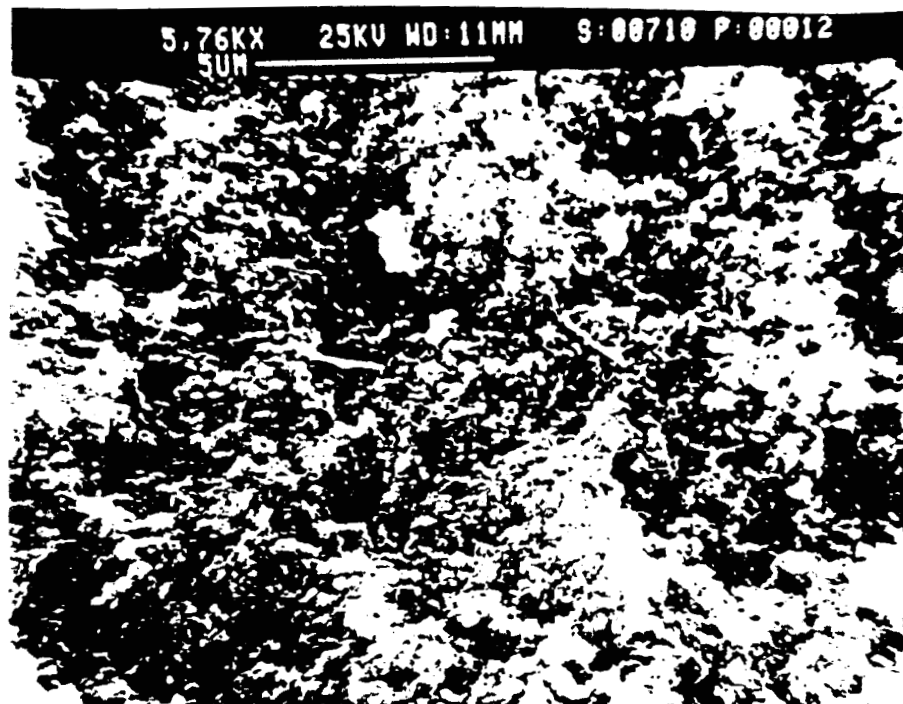
a. 100% N_2 atmosphere
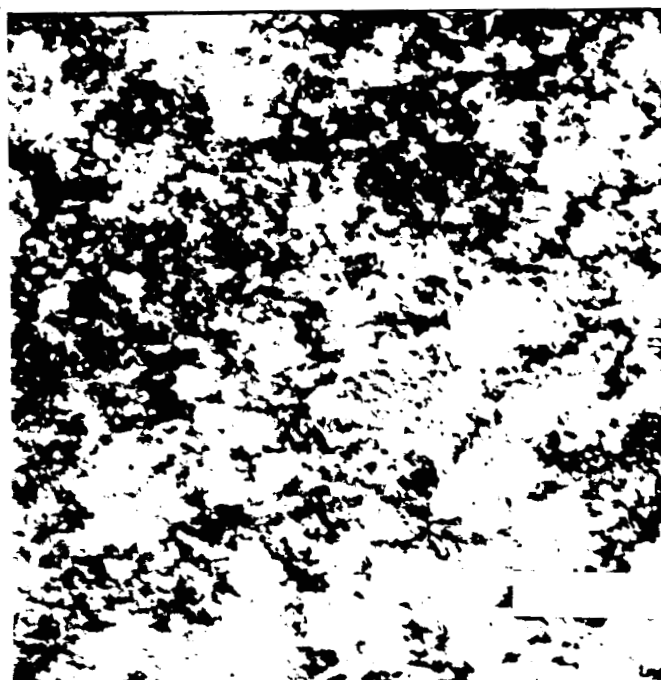
b. 4 vol% H_2/N_2 atmosphere (bar = 5μ)

Figure 13: RBSN microstructure, nitrided at 1200"C for 24 hr.

Figure 14: Representative fiber/matrix region in RBSN samples before sintering.

Figure 15: Low additive concentration RBSN, HIP'd at 1450°C.
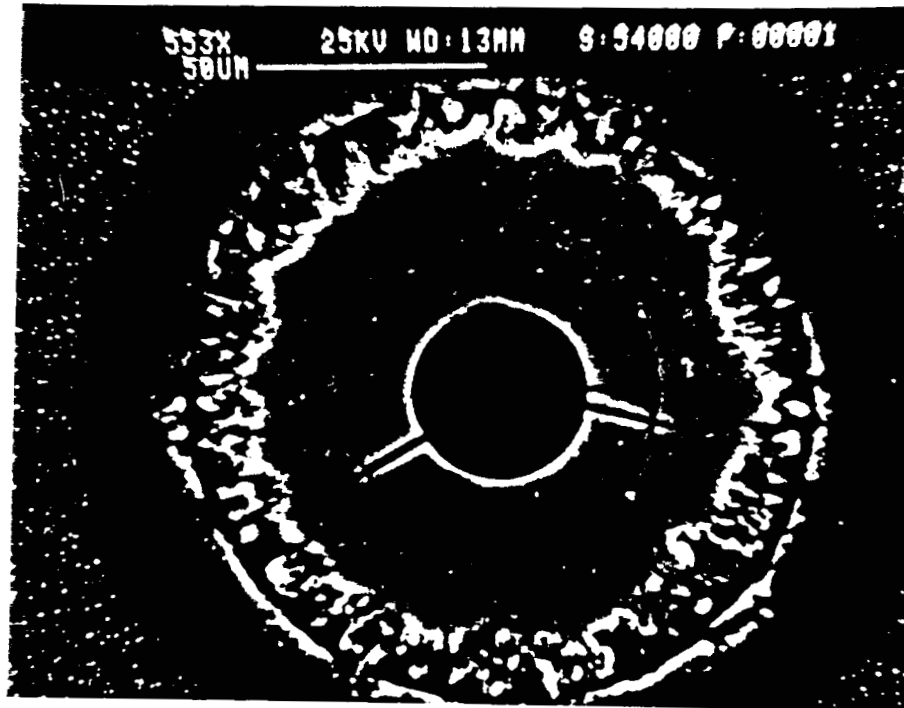
Figure 16: RBSN with 6.0 wt% MgO, HIP'd at 1600"C.

a. HIP'd at 1400°C
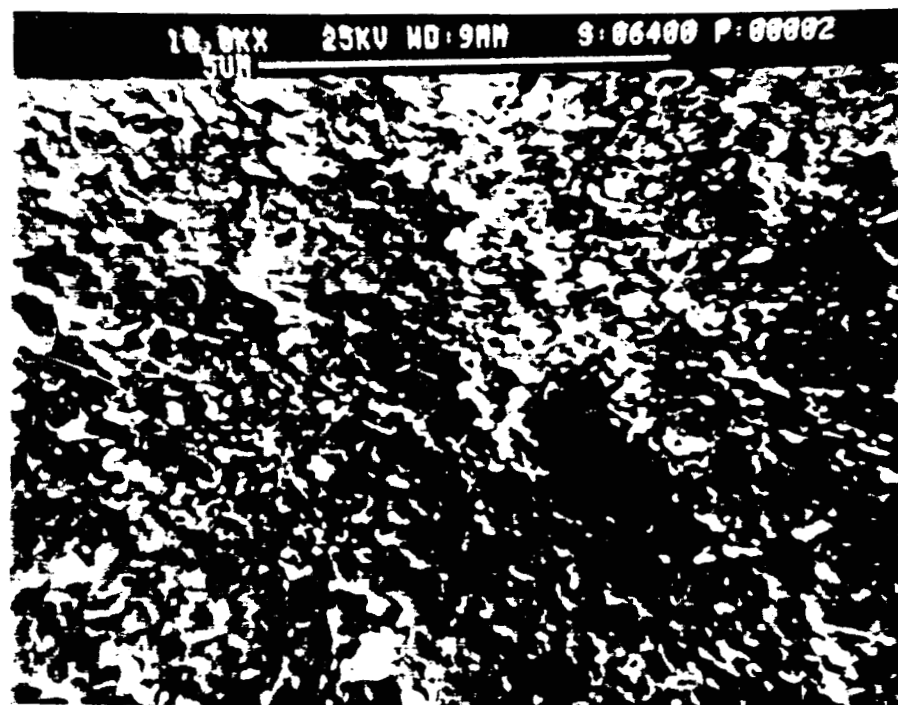
b. HIP'd at 1450"C

Figure 17: Microstructure of high additive concentration RBSN, densified at two different temperatures.
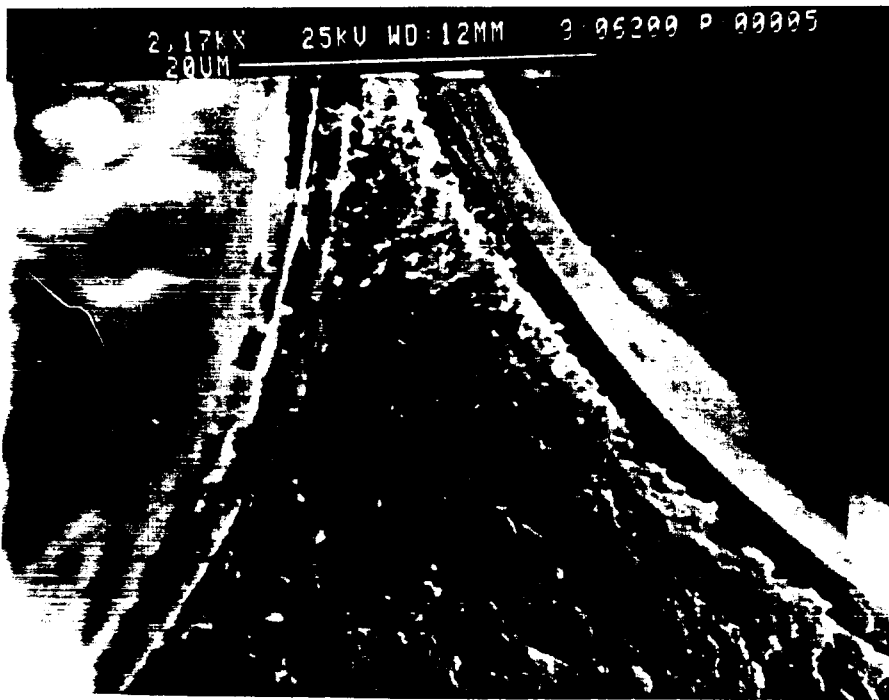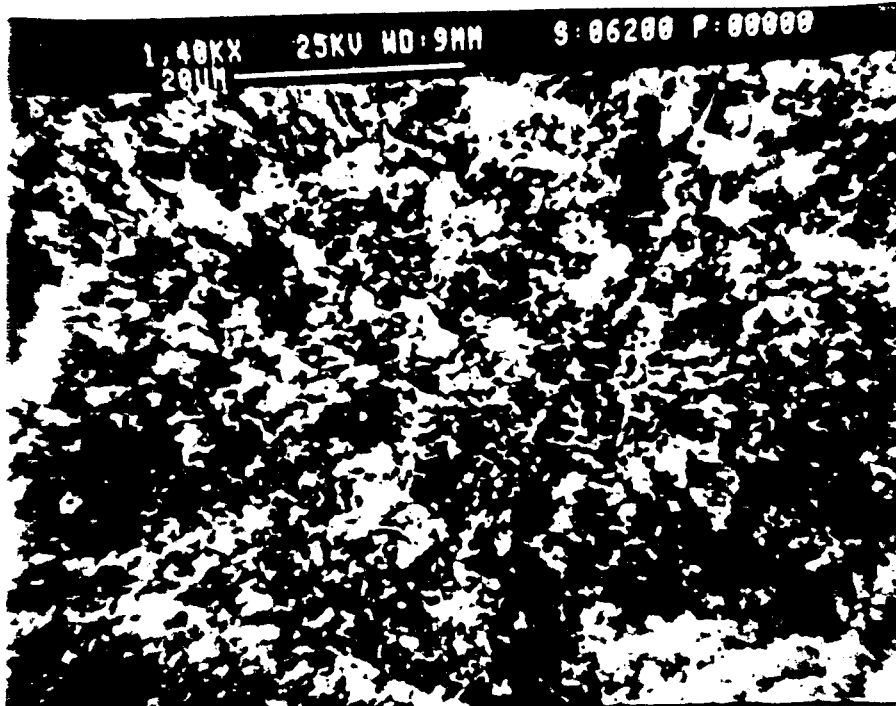
Figure 18: Photomicrographs exhibiting the inhomogeneous nature of the HIP'd RBSN microstructure (high additive conc., 1400°C).
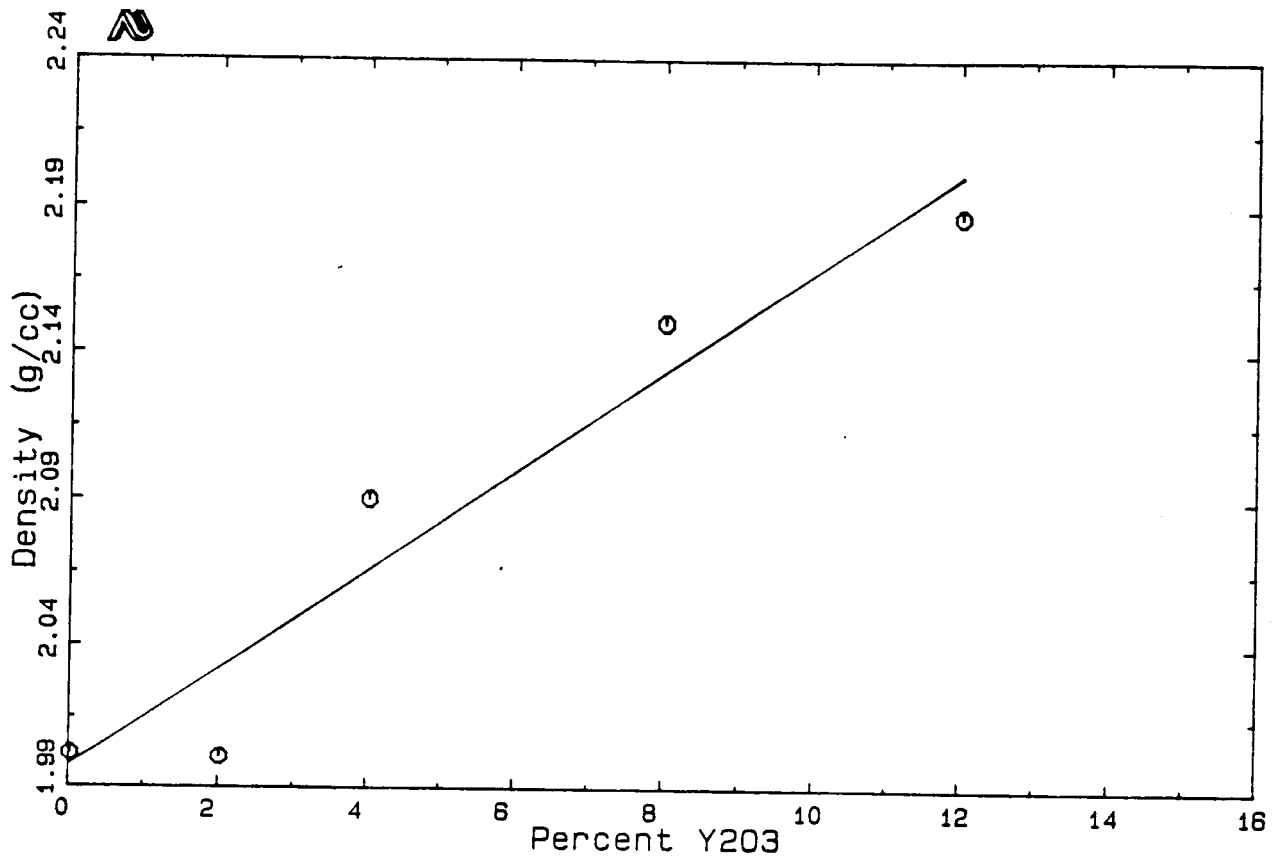
Figure 19: Density vs. wt% Y_2O_3 for the nitrided Matrix 2 samples.
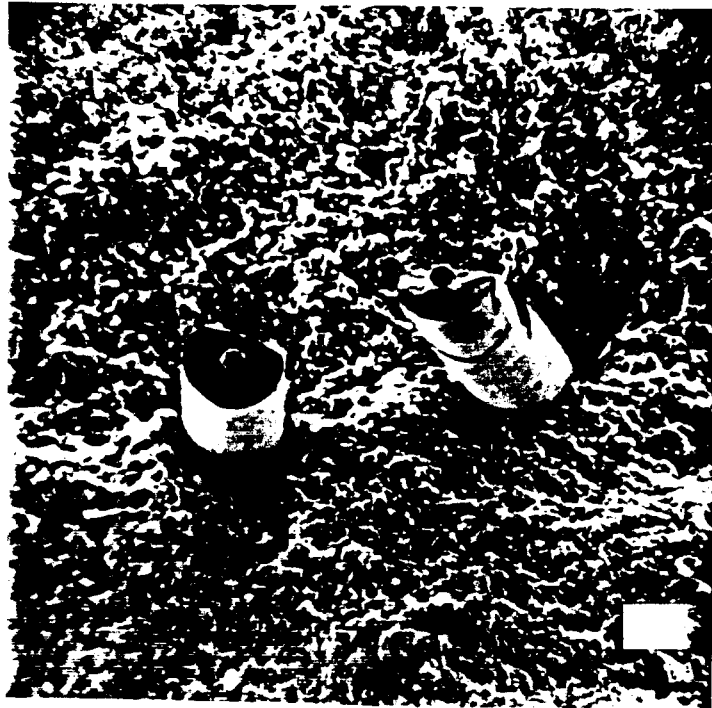
Figure 20: Representative RBSN microstructure of Matrix 2 samples, prior to pressureless sintering (bar = 100μ).
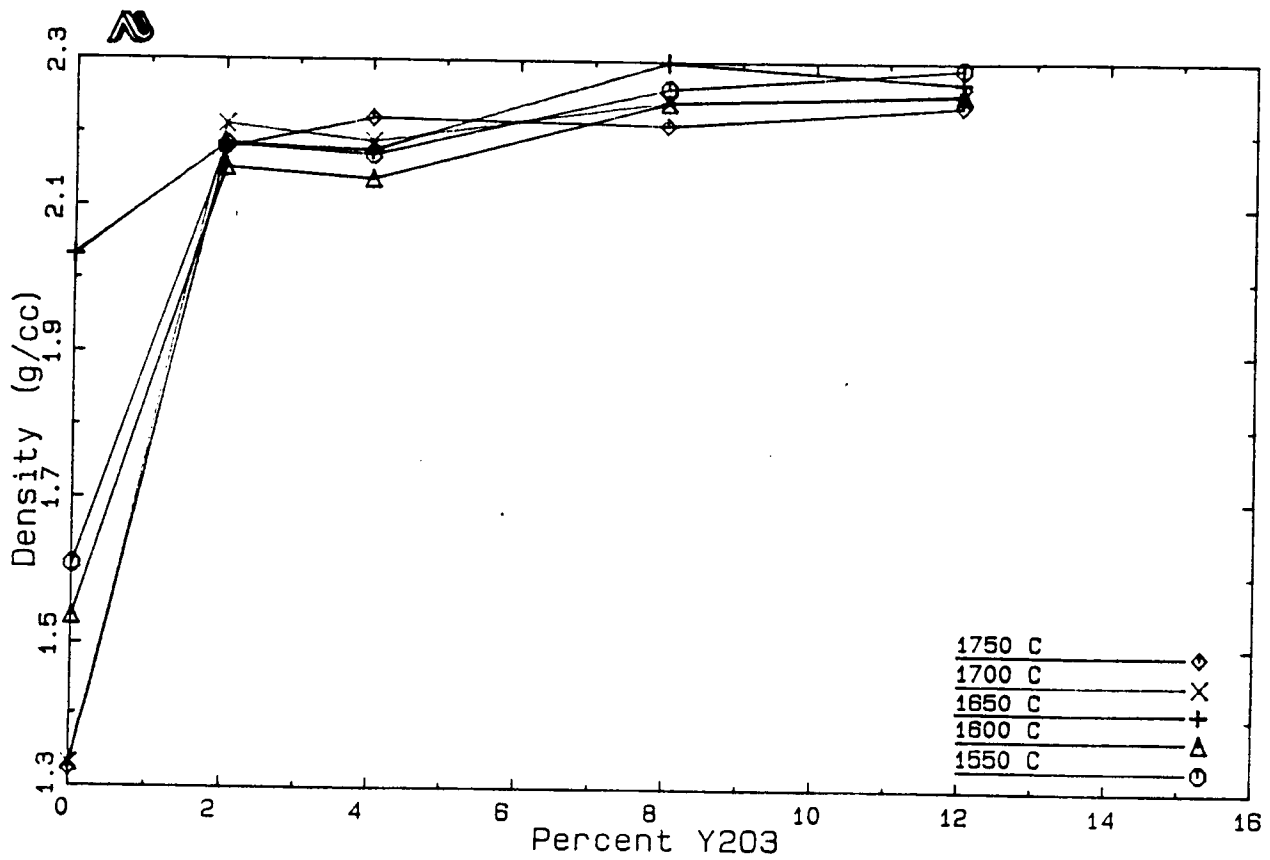
Figure 21: Density vs. wt% Y_2O_3 for various sintering temperatures (Matrix 2 samples).

a. (bar = 20μ)
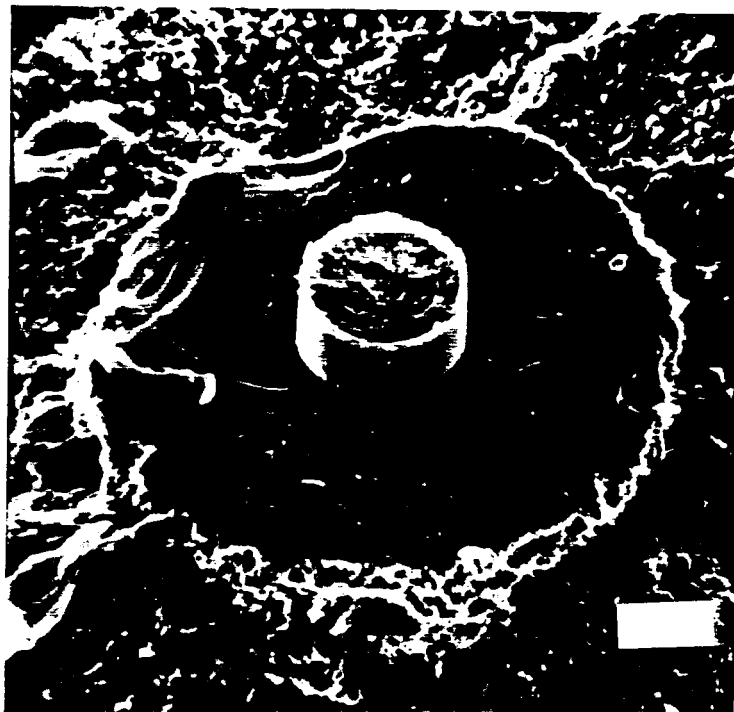
b. (bar = 20μ)

Figure 22: Microstructure of pressureless sintered RBSN (1550"C) showing the limited fiber/matrix interaction.
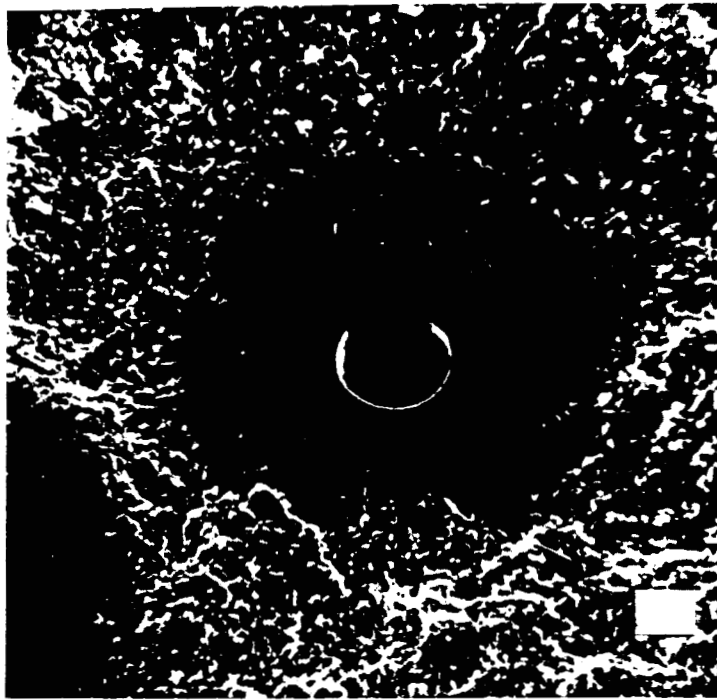
a. Flat fracture (bar = 20μ)


b. Fracture mirrors (bar= 50μ)

Figure 23: Microstructure of pressureless sintered RBSN (1750"C) showing extensive fiber/matrix interaction.

a. Starck H-1 (bar = 5μ)
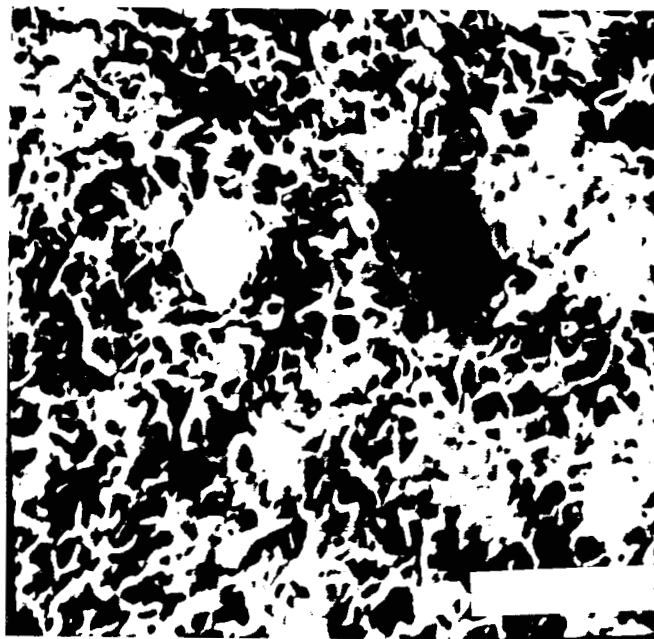
b. Ube SN-E-10 (bar = 4μ)

Figure 24: Microstructure of hot-pressed Si_3N_4 powders (Matrix 3).
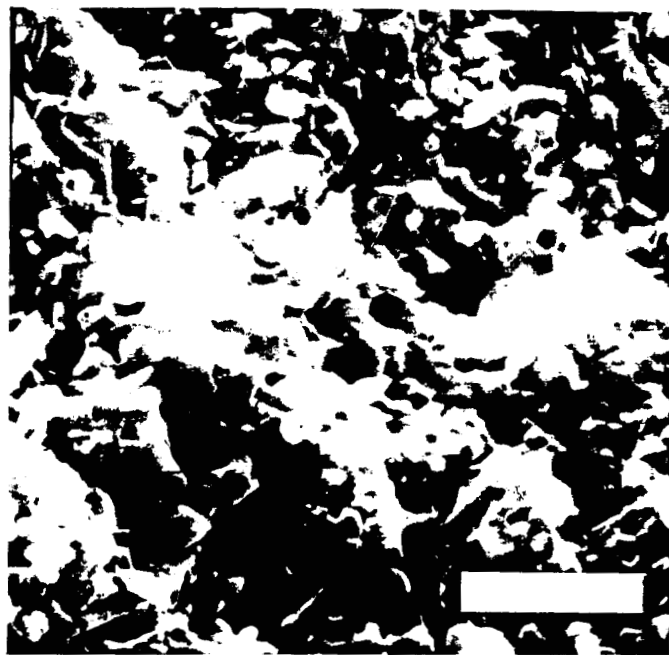
a. KemaNord P95 (bar = 4μ)
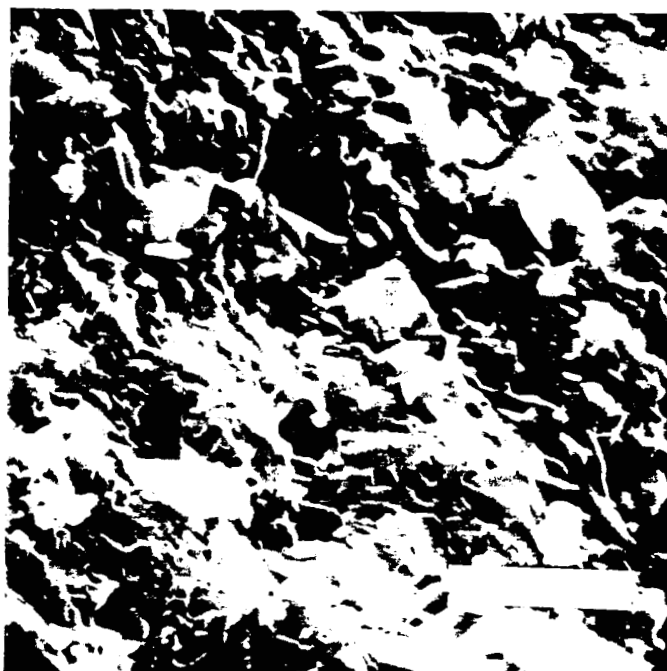
b. KemaNord S95 (bar = 4μ)

Figure 25: Microstructure of hot-pressed Si_3N_4 powders (Matrix 3).

a. (bar = 20μ)
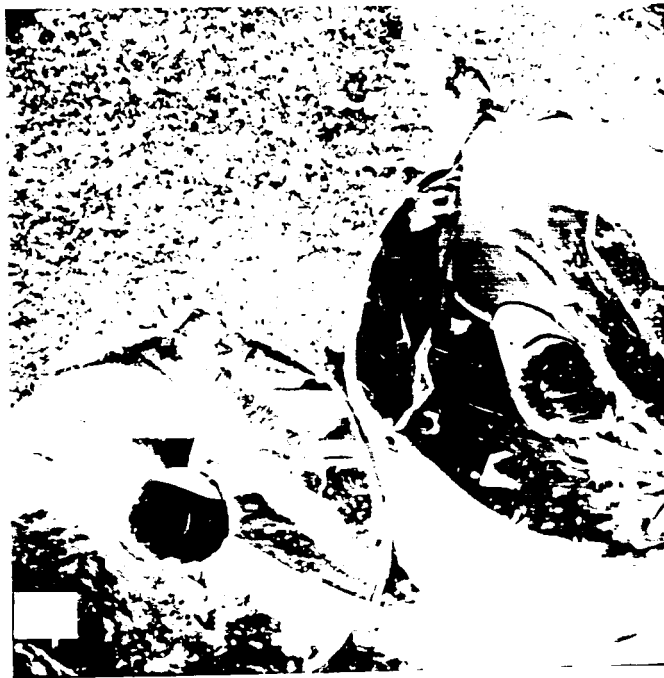
b. (bar = 20μ)

Figure 26: Photomicrograph showing the limited fiber/matrix interaction in the hot-pressed Si_3N_4 (Matrix 3).

Appendix A

Literature Values: Hardness and Toughness of Si_3N_4

Measurement Technique	Hardness (H) (GPa)	Toughness (K_c) (MPa m$^{1/2}$)	Additional Information
Chevron-notch[47]		4.68	Hot-pressed NC-132 (Norton Co.)
Notched-beam[48]		2.32	RBSN (expt.)
4-point bend[49]		1.5	RBSN (expt.)
4-point bend[50]		4.5	Hot-pressed HS-130 (Norton Co.)
Double Torsion[45]	16	5	Hot-pressed NC-132
Vickers Indent[52]	16.5	5.1	Hot-pressed NC-132
Vickers Indent[52]	8.4	3.1	RBSN NC-350 (Norton Co.)
Vickers Indent[51]	14.1	4.9	Hot-pressed with MgO (Norton Co.)

Appendix B

Si$_3$N$_4$ Powder Specifications

Supplier-Grade	Fe (wt %)	Al (wt %)	O (wt %)	α/β ratio	Surface Area BET (m^2/g)
Ube: SN-E-10	$\leq$0.01	$\leq$0.01	$\leq$2.0	95/5	10
Starck: H-1	$\leq$0.08	$\leq$0.20	$\leq$1.4	94/6	8.5
KemaNord: P95	$\leq$0.07	$\leq$0.03	$\leq$1.5	92/8	11
KemaNord: S95	$\leq$0.25	$\leq$0.11	$\leq$1.3	91/9	9.9

Appendix C

Matrix 1 Data - HIP'd SRBSN

N_2 Nitriding Atmosphere				
SAMPLE ID	Sintering Temp ("C)	Density (g/cc)	Hardness (H) (GPa)	Toughness (K_c) (MPa m$^{1/2}$)
High Y_2O_3	Nitrided	1.61	0.45	0.20
High Y_2O_3	1400	2.49	0.90	0.62
High Y_2O_3	1450	2.49	0.84	0.40
Low Y_2O_3	Nitrided	1.48	0.57	0.31
Low Y_2O_3	1400	2.35	0.58	0.32
Low Y_2O_3	1450	2.35	0.57	0.32

$N_2/4$ vol%H_2 Nitriding Atmosphere				
SAMPLE ID	Sintering Temp ("C)	Density (g/cc)	Hardness (H) (GPa)	Toughness (K_c) (MPa m$^{1/2}$)
High Y_2O_3	Nitrided	2.43	0.76	0.57
High Y_2O_3	1350	2.46	0.71	0.54
High Y_2O_3	1400	2.48	0.82	0.61
High Y_2O_3	1450	2.51	0.80	0.51
Low Y_2O_3	Nitrided	2.34	0.73	0.57
Low Y_2O_3	1350	2.36	0.71	0.46
Low Y_2O_3	1400	2.32	0.71	0.42
Low Y_2O_3	1450	2.37	0.67	0.34

Appendix D

Matrix 2 Data - Pressureless Sintered RBSN

Weight % Y_2O_3	Sintering Temp ("C)	Density (g/cc)	Hardness (H) (GPa)	Toughness (K_c) (MPa m$^{1/2}$)
0		2.00	0.10	0.16
2.0		2.00	0.10	0.16
4.0	Nitrided	2.10	0.11	0.18
8.0		2.15	0.12	0.19
12.0		2.19	0.14	0.21
0		1.61	0.34	0.40
2.0		2.18	0.39	0.34
4.0	1550	2.17	0.40	0.37
8.0		2.26	0.42	0.39
12.0		2.29	0.38	0.34
0		1.54	0.33	0.35
2.0		2.15	0.38	0.37
4.0	1600	2.14	0.36	0.34
8.0		2.24	0.35	0.36
12.0	.	2.26	0.38	0.35
0		2.03	0.33	0.33
2.0		2.18	0.43	0.37
4.0	1650	2.18	0.37	0.37
8.0		2.30	0.44	0.34
12.0		2.27	0.47	0.34
0		1.33	0.07	0.13
2.0		2.21	0.28	0.32
4.0	1700	2.19	0.42	0.38
8.0		2.24	0.50	0.46
12.0		2.25	0.34	0.40
0		1.32	0.06	0.10
2.0		2.18	0.36	0.35
4.0	1750	2.22	0.52	0.48
8.0		2.21	0.40	0.40
12.0		2.24	0.37	0.36

Appendix E

Matrix 3 Data - Hot-Pressed Si_3N_4

Samples Hot-Pressed with NASA Sintering Composition				
Si_3N_4 Powder	Density (g/cc)	Hardness (H) (GPa)	Toughness (K_c) (MPa $m^{1/2}$)	Statistical Variance (μ^2)
Starck H-1	2.94	1.47	1.46	15.58
Ube SN-E-10	2.87	1.51	1.36	1.92
KemaNord P95	3.00	1.69	1.80	0.65
KemaNord S95	3.10	1.73	0.80	0.27

Samples Hot-Pressed with Y-SiAlON Sintering Composition				
Si_3N_4 Powder	Density (g/cc)	Hardness (H) (GPa)	Toughness (K_c) (MPa $m^{1/2}$)	Statistical Variance(μ^2)
Starck H-1	2.81	0.93	1.57	3.18
KemaNord P95	2.92	1.21	1.39	0.93
KemaNord S95	3.00	1.38	0.89	0.79